Oxygen Transport Ceramic Membranes

Quarterly Report

October 2006 – December 2006

Principal Authors:

Prof. S. Bandopadhyay

Dr. T. Nithyanantham

Issued: February 2007

DOE Award # DE-FC26-99FT40054

University of Alaska Fairbanks
Fairbanks, AK 99775

Contributing Authors:

1. **Y-W. Sin and H. U. Anderson,** Materials Research Center, University of Missouri-Rolla, Rolla, MO 65401
2. **Prof. Alan Jacobson and Prof. C.A. Mims;** University of Houston/University of Toronto

DISCLAIMER

This report was prepared as an account of the work sponsored by an agency of the United States Government. Neither the United States Government nor any agency thereof, nor any of their employees, makes any warranty, express or implied, or assumes any legal liability or responsibility for the accuracy, completeness, or usefulness of any information, apparatus, product, or process disclosed, or represents that its use would not infringe privately owned rights. Reference herein to any specific commercial product, process, or service by trade name, trademark, manufacturer, or otherwise does not necessarily constitute or imply its endorsement, recommendation, or favoring by the United States Government or any agency thereof. The views and opinions of authors expressed herein do not necessarily state or reflect those of the United States Government or any agency thereof.

ABSTRACT

Ti doping on $La_{1-x}Sr_xFeO_{3-\delta}$ (LSF) tends to increase the oxygen equilibration kinetics of LSF in lower oxygen activity environment because of the high valence state of Ti. However, the addition of Ti decreases the total conductivity because the acceptor ($[Sr'_{La}]$) is compensated by the donor ($[Ti^{\bullet}_{Fe}]$) which decreases the carrier concentration. The properties of $La_{0.2}Sr_{0.8}Fe_{1-x}Ti_xO_{3-\delta}$ (LSFT, x = 0.45) have been experimentally and theoretically investigated to elucidate (1) the dependence of oxygen occupancy and electrochemical properties on temperature and oxygen activity by thermogravimetric analysis (TGA) and (2) the electrical conductivity and carrier concentration by Seebeck coefficient and electrical measurements.

In the present study, dual phase ($La_{0.2}Sr_{0.8}Fe_{0.6}Ti_{0.4}O_{3-\delta}/Ce_{0.9}Gd_{0.1}O_{2-\delta}$) membranes have been evaluated for structural properties such as hardness, fracture toughness and flexural strength. The effect of high temperature and slightly reducing atmosphere on the structural properties of the membranes was studied. The flexural strength of the membrane decreases upon exposure to slightly reducing conditions at 1000°C. The as-received and post-fractured membranes were characterized using XRD, SEM and TG-DTA to understand the fracture mechanisms. Changes in structural properties of the composite were sought to be correlated with the physiochemical features of the two-phases.

We have reviewed the electrical conductivity data and stoichiometry data for $La_{0.2}Sr_{0.8}Cr_{0.2}Fe_{0.8}O_{3-\delta}$ some of which was reported previously. Electrical conductivity data for $La_{0.2}Sr_{0.8}Cr_{0.2}Fe_{0.8}O_{3-\delta}$ (LSCrF) were obtained in the temperature range, 752 ~ 1055 °C and in the pO_2 range, 10^{-18} ~ 0.5 atm. The slope of the plot of log σ vs. log pO_2 is ~1/5 in the p-type region, $pO_2 = 10^{-5} \sim 10^{-1}$ atm. The pO_2 at which the p-n transition is observed increases with increasing temperature. The activation energy for ionic conduction was estimated to be 0.86 eV from an Arrhenius plot of the minimum conductivity vs. reciprocal temperature. At temperatures below 940°C, a plateau in the conductivity isotherm suggests the presence of a two-phase region. Most likely, phase separation occurs to form a mixture of a perovskite phase and an oxygen vacancy ordered phase related to brownmillerite. Additional data for the oxygen non stoichiometry are presented.

TABLE OF CONTENTS

INTRODUCTION		1
EXECUTIVE SUMMARY		3
Task 1	Preparation and Characterization of Dense Ceramic oxygen Permeable Membranes	4
Task 2	Determine material mechanical properties under conditions of high temperature and reactive atmosphere	16
Task 3	Measurement of Surface Activation/Reaction rates in Ion Transport Membranes using Isotope Tracer and Transient Kinetic Techniques	29
CONCLUSIONS		36
LISTS OF ACRONYMS AND ABBREVIATIONS		37
REFERENCES		38

LIST OF GRAPHICAL MATERIALS

Figure 1. σ vs. pO_2 of $La_{0.2}Sr_{0.8}TiO_3$ at 800°C (annealing temperature was 1200°C.)

Figure 2. Conductivity of LSF as a function of temperature in air

Figure 3. XRD profiles of LSFT annealed in forming gas (10% H_2 / 90% N_2) at 1000°C [1]

Figure 4. XRD profiles of LSFT annealed at 600, 1200, 1300, and 1400°C

Figure 5. Oxygen occupancy (3-δ) of LSFT as function of oxygen activity at 1200°C

Figure 6. Stoichiometry of $La_{0.2}Sr_{0.8}Fe_{0.55}Ti_{0.45}O_{3-\delta}$ (LSFT) [2]

Figure 7. Weight changes of LSFT as a function of oxygen activity at 1200°C

Figure 8. Total conductivity and Seebeck coefficient of LSFT as a function of temperature.

Figure 9. Charge carrier concentration and Seebeck coefficient of LSFT as a function of temperature

Figure 10 Net acceptor dopant concentration and Seebeck coefficient of LSFT as a function of temperature

Figure 11. σ vs. 1/T of LSFT and corresponding mobility measured in air as a function of temperature

Figure 12. Electrical conductivity as a function of oxygen activity of LSFT at 1000 and 1200°C.

Figure 13. Log σ vs. Po_2 of dense $Sr_{0.9}Ti_{0.6}Fe_{0.4}O_{3-\delta}$ (sintered at 1600°C) at 800°C [2]

Figure 14. Seebeck coefficient vs. Log Po_2 of ~ 50% dense $La_{0.2}Sr_{0.8}Fe_{0.55}Ti_{0.45}O_{3-\delta}$ (LSFT) at 900°C

Figure 15. Back scattered SEM micrographs of the 'as-received' LSFT-CGO membranes. The dark phase is LSFT and the bright phase is CGO. Percolation of the two-phases is clearly observed in (a) and no micro cracks and any other flaws caused by the thermal expansion mismatch are visible at the grain boundaries (b).

Figure 16. The XRD patterns for LSFT-CGO membranes.

Figure 17. Change in weight for LSFT-CGO in air and N_2 environment.

Figure 18. Dependence of the hardness (a) and Fracture toughness (b) of dual phase membranes on indentation load

Figure 19. The crack propagation behavior of dual phase membrane. The dependence of L/a on indentation load indicates the presence of some toughening mechanisms in the membrane.

Figure 20 Effect of temperature and environment on the flexural strength of the dual phase membrane

Figure 21. SEM micrographs of fracture surfaces at room temperature (a) and at 1000°C in N_2 (b) Fracture was mainly transgranular at the room temperature and intergranular at 1000°C in N_2 atmosphere.

Figure 22. Change in weight of the LSFT-CGO in air. The weight gain of the membrane during TGA in air not only indicates non-stoichiometry of the membrane during the strength test but also implies that the membrane remain oxygen deficient even after the strength test.

Figure 23. Back scattering electron micrograph of a crack path. The arrow mark shows the direction of crack propagation. The darker grains are LSFT and brighter grains are CGO. Note the crack prefers the boundaries of LSFT and cleaves CGO on its course.

Figure 24. pO_2 dependence of electrical conductivities at 752, 802, 854, 902, 942, 985, 1024, and 1055°C.

Figure 25. pO_2 dependence of electrical conductivities in the $pO_2 = 10^{-5} \sim 10^{-1}$ atm

Figure 26. The temperature dependence of p-n transition behavior

Figure 27. Comparison of conductivity isotherms according to the direction: "high to low pO_2" run and "low to high pO_2" run. For clarity, "high to low pO_2" runs are offset.

INTRODUCTION

Conversion of natural gas to liquid fuels and chemicals is a major goal for the Nation as it enters the 21st Century. Technically robust and economically viable processes are needed to capture the value of the vast reserves of natural gas on Alaska's North Slope, and wean the Nation from dependence on foreign petroleum sources. Technologies that are emerging to fulfill this need are all based syngas as an intermediate. Syngas (a mixture of hydrogen and carbon monoxide) is a fundamental building block from which chemicals and fuels can be derived. Lower cost syngas translates directly into more cost-competitive fuels and chemicals.

The currently practiced commercial technology for making syngas is either steam methane reforming (SMR) or a two-step process involving cryogenic oxygen separation followed by natural gas partial oxidation (POX). These high-energy, capital-intensive processes do not always produce syngas at a cost that makes its derivatives competitive with current petroleum-based fuels and chemicals.

In the mid 80's BP invented a radically new technology concept that will have a major economic and energy efficiency impact on the conversion of natural gas to liquid fuels, hydrogen, and chemicals.[1] This technology, called Electropox, integrates oxygen separation with the oxidation and steam reforming of natural gas into a single process to produce syngas with an economic advantage of 30 to 50 percent over conventional technologies.[2]

The Electropox process uses novel and proprietary solid metal oxide ceramic oxygen transport membranes [OTMs], which selectively conduct both oxide ions and electrons through their lattice structure at elevated temperatures.[3] Under the influence of an oxygen partial pressure gradient, oxygen ions move through the dense, nonporous membrane lattice at high rates with 100 percent selectivity. Transported oxygen reacts with natural gas on the fuel side of the ceramic membrane in the presence of a catalyst to produce syngas.

In 1997 BP entered into an OTM Alliance with Praxair, Amoco, Statoil and Sasol to advance the Electropox technology in an industrially sponsored development program. These five companies

---

[1]Mazanec, T. J.; Cable, T. L.; Frye, J. G., Jr.; US 4,793,904, 27 Dec **1988**, assigned to The Standard Oil Company (now BP America), Mazanec, T. J.; Cable, T. L.; US 4,802,958, 7 Feb **1989**, assigned to the Standard Oil Co. (now BP America), Cable, T. L.; Mazanec, T. J.; Frye, J. G., Jr.; European Patent Application 0399833, 24 May **1990**, published 28 November **1990.**

[2]Bredesen, R.; Sogge, J.; "A Technical and Economic Assessment of Membrane Reactors for Hydrogen and Syngas Production" presented at Seminar on the Ecol. Applic. of Innovative Membrane Technology in the Chemical Industry", Cetraro, Calabria, Italy, 1-4 May **1996**.

[3] Mazanec, T.J., *Interface*, **1996**; Mazanec, T.J., *Solid State Ionics*, 70/71, **1994** 11-19; "Electropox: BP's Novel Oxidation Technology", T.J. Mazanec, pp 212-225, in "The Role of Oxygen in Improving Chemical Processes", M. Fetizon and W.J. Thomas, eds, Royal Society of Chemistry, London, **1993**; "Electropox: BP's Novel Oxidation Technology", T.J. Mazanec, pp 85-96, in "The Activation of Dioxygen and Homogeneous Catalytic Oxidation", D.H.R. Barton, A. E. Martell, D.T. Sawyer, eds, Plenum Press, New York, **1993**; "Electrocatalytic Cells for Chemical Reaction", T.J. Mazanec, T.L. Cable, J.G. Frye, Jr.; Prep Petrol Div ACS, San Fran, **1992** *37*, 135-146; T.J. Mazanec, T.L. Cable, J.G. Frye, Jr.; *Solid State Ionics*, **1992**, 53-56, 111-118.

have been joined by Phillips Petroleum and now are carrying out a multi-year $40+ million program to develop and commercialize the technology. The program targets materials, manufacturing and engineering development issues and culminates in the operation of semi-works and demonstration scale prototype units.

The Electropox process represents a truly revolutionary technology for conversion of natural gas to synthesis gas not only because it combines the three separate unit operations of oxygen separation, methane oxidation and methane steam reforming into a single step, but also because it employs a chemically active ceramic material in a fundamentally new way. On numerous fronts the commercialization of Electropox demands solutions to problems that have never before been accomplished. Basic problems in materials and catalysts, membrane fabrication, model development, and reactor engineering all need solutions to achieve commercial success. Six important issues have been selected as needing understanding on a fundamental level at which the applied Alliance program cannot achieve the breadth and depth of understanding needed for rapid advancement. These issues include:

1. Oxygen diffusion kinetics (University of Houston);
2. Phase stability and stress development (University of Missouri - Rolla);
3. Mechanical property evaluation in thermal and chemical stress fields (University of Alaska Fairbanks)

Statement of Work

Task 1 *Evaluate phase stability and thermal expansion of candidate perovskite membranes and develop techniques to support these materials on porous metal structures.*

Task 2 *Determine materials mechanical properties under conditions of high temperatures and reactive atmospheres.*

Task 3 *Measure kinetics of oxygen uptake and transport in ceramic membrane materials under commercially relevant conditions using isotope labeling techniques.*

EXECUTIVE SUMMARY

LSFT not only exhibits p-type in the high oxygen activity regime, but also has an n-type in the reducing atmosphere. Higher concentrations of oxygen vacancies in the low oxygen activity regime may improve the performance of LSFT as an OTM. The hole concentration is related to the difference in the acceptor and donor concentration by the relation $p = [Sr'_{La}] - [Ti^{\bullet}_{Fe}]$. The chemical formulation predicts that the hole concentration is, p = 0.8-0.45 or 0.35. Experimental measurements indicated that p is about ~ 0.35. The activation energy of conduction is 0.2 eV which implies that the LSCF conducts via the small polaron conduction mechanism.

The dual phase membranes have been evaluated for structural properties. An increasing crack growth resistance was observed for the membranes heat-treated at 1000°C in air and N_2 with increasing crack length. The flexural strength was evaluated to be 104 MPa and 51.2 MPa for dual phase membranes in room temperature (in air) and at 1000°C in N_2 respectively. The oxygen deficiency in LSFT caused by the N_2 atmosphere at 1000°C is thought to promote intergranular debonding during crack propagation and observed transgranular fracture. Further studies can elucidate on the role of chemical expansion on mechanical properties of dual phase membranes.

We have reviewed the electrical conductivity data and stoichiometry data for $La_{0.2}Sr_{0.8}Cr_{0.2}Fe_{0.8}O_{3-\delta}$ some of which was reported previously. Electrical conductivity data for $La_{0.2}Sr_{0.8}Cr_{0.2}Fe_{0.8}O_{3-\delta}$ (LSCrF) were obtained in the temperature range, 752 ~ 1055 °C and in the pO_2 range, 10^{-18} ~ 0.5 atm. The slope of the plot of log σ vs. log pO_2 is ~1/5 in the p-type region, $pO_2 = 10^{-5} \sim 10^{-1}$ atm. The pO_2 at which the p-n transition is observed increases with increasing temperature. The activation energy for ionic conduction was estimated to be 0.86 eV from an Arrhenius plot of the minimum conductivity vs. reciprocal temperature. At temperatures below 940°C, a plateau in the conductivity isotherm suggests the presence of a two-phase region. Most likely, phase separation occurs to form a mixture of a perovskite phase and an oxygen vacancy ordered phase related to brownmillerite. Non equilibrium effects are observed but unlike those in LSFTO, they become less apparent with increasing temperature.

Task 1: Preparation and Characterization of Dense Ceramic oxygen Permeable Membranes

Yong-Wook Sin and H. U. Anderson

Materials Research Center, University of Missouri-Rolla, Rolla, MO 65401

Conductivity and Seebeck coefficient of $La_{0.2}Sr_{0.8}Fe_{0.55}Ti_{0.45}O_{3-\delta}$ (LSFT) as a function of temperature

Summary

Ti doping on $La_{1-x}Sr_xFeO_{3-\square}$ (LSF) tends to increase the oxygen equilibration kinetics of LSF in lower oxygen activity environment because of the high valence state of Ti. However, the addition of Ti decreases the total conductivity because the acceptor ($[Sr_{La}^{'}]$) is compensated by the donor ($[Ti_{Fe}^{\bullet}]$) which decreases the carrier concentration. The properties of $La_{0.2}Sr_{0.8}Fe_{1-x}Ti_xO_{3-\square}$ (LSFT, x = 0.45) have been experimentally and theoretically investigated to elucidate (1) the dependence of oxygen occupancy and electrochemical properties on temperature and oxygen activity by thermogravimetric analysis (TGA) and (2) the electrical conductivity and carrier concentration by Seebeck coefficient and electrical measurements.

$SrTiO_3$ (perovskite, ABO_3), an n-type conductor, has thermodynamic stability, but exhibits low electronic and ionic conductivity at high of temperature and high oxygen activity. La doping on the A-site of $SrTiO_3$ does provide increased electrical conductivity in highly reducing atmospheres (Figure 1). Acceptor doping such as Fe on the B-site of $SrTiO_3$ provides p-type conduction and decreases electrical conductivity. On the other hand, ferrite such as $(La, Sr)FeO_{3-\square}$ (LSF) which is known as a mixed ionic and p type electronic conductor is currently being widely used because of its high electronic conductivity in oxidizing conditions, but in low oxygen activity its conductivity is suppressed (Figure 2). When high valence state elements like Ti are added as a donor on the B site of LSF, the electrical conductivity at lower oxygen activity tends to be increased. Therefore, Ti doped $(La, Sr)FeO_{3-\square}$, may attain high electronic, ionic conductivity as well as improved stability in highly reducing atmospheres. As shown in

Figure 3 [1], according to the XRD results, the perovskite structure in LSFT was also preserved very well after 12 hours at 1000°C in 10% H_2 / 90% N_2 .

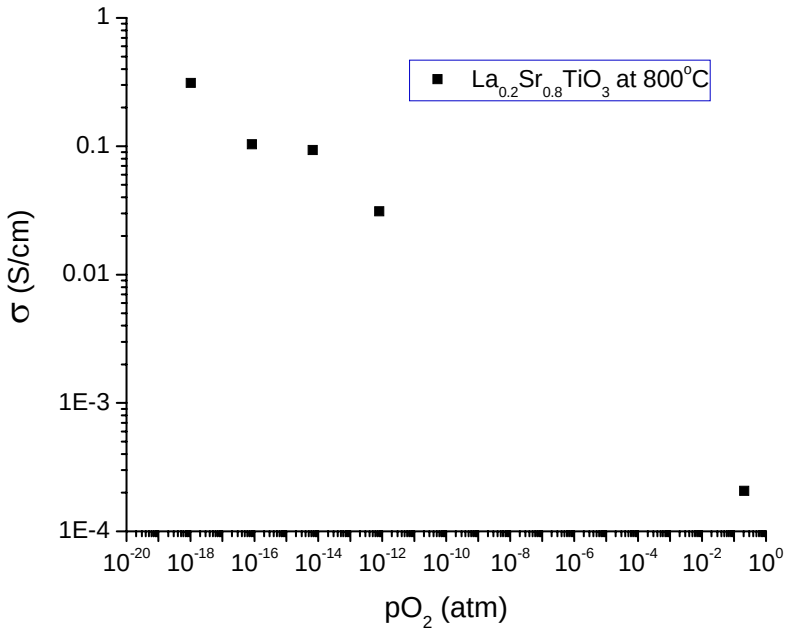

Figure 1 σ vs. pO_2 of $La_{0.2}Sr_{0.8}TiO_3$ at 800°C (annealing temperature was 1200°C.)

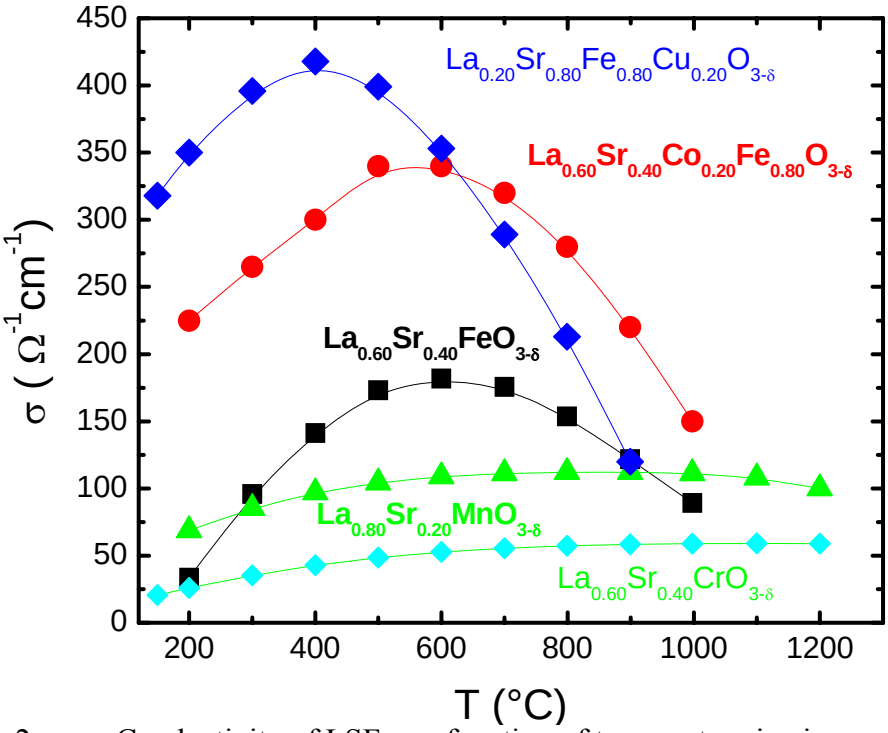

Figure 2 Conductivity of LSF as a function of temperature in air

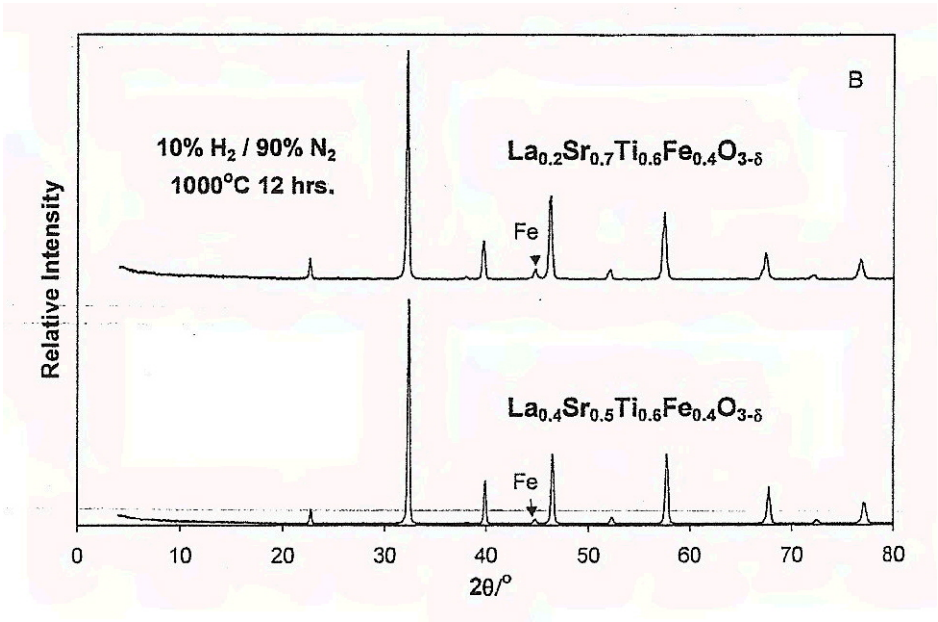

Figure 3 XRD profiles of LSFT annealed in forming gas (10% H_2 / 90% N_2) at 1000°C [1]

Results and Discussion

1. LSFT Powder Preparation

The first objective was to fabricate well dispersed and nano-sized LSFT powder. To achieve this goal, the development of powder preparation technologies to fabricate non-agglomerated, nano-sized powder was required. Several water based solution processes were investigated to prepare the required powder. Among them, the method using ethylene glycol and nitrates was selected as the best route for power preparation. LSFT powder samples were annealed at 600, 1200, 1300 and 1400°C and characterized by using XRD. As can be seen in the Figure 4, the XRD profiles show that resulting LSFT was single phase with the perovskite structure.

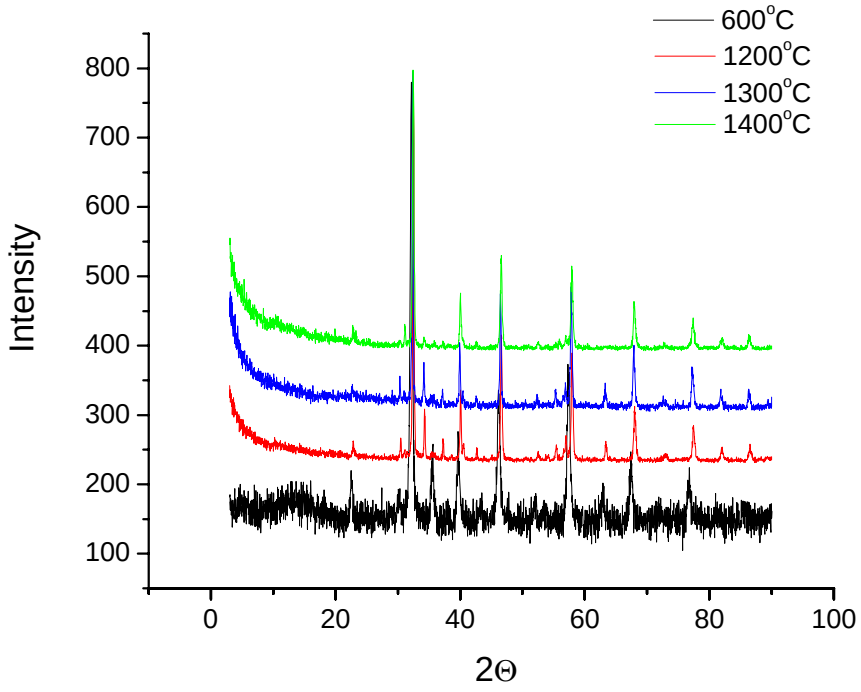

Figure 4 XRD profiles of LSFT annealed at 600, 1200, 1300, and 1400°C

2. Oxygen Occupancy Study

Based on the assumption that the structure had full oxygen occupancy at room temperature in air, the oxygen occupancy (3-δ) as a function of oxygen activity was estimated by thermogravimetric analysis (TGA). This assumption yielded the oxygen occupancy (3-δ) at 1200°C to be 2.92 in air, and 2.86 in 1 x 10^{-12} atm (Figure 5).

These data agree with that found the University of Houston (Figure 6) [2]. As shown in Figure 7, below 1 x 10^{-13} atm of oxygen activity at 1200°C, the LSFT lost weight due to dissociation. However, upon re-oxidation, the weight loss was found to be fullyreversible.

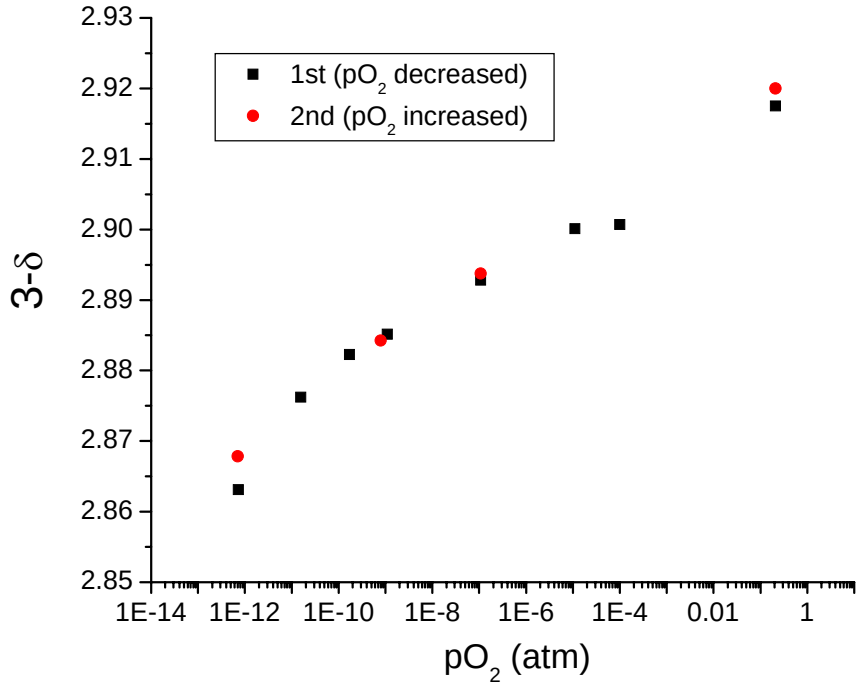

Figure 5 Oxygen occupancy (3-δ) of LSFT as function of oxygen activity at 1200°C

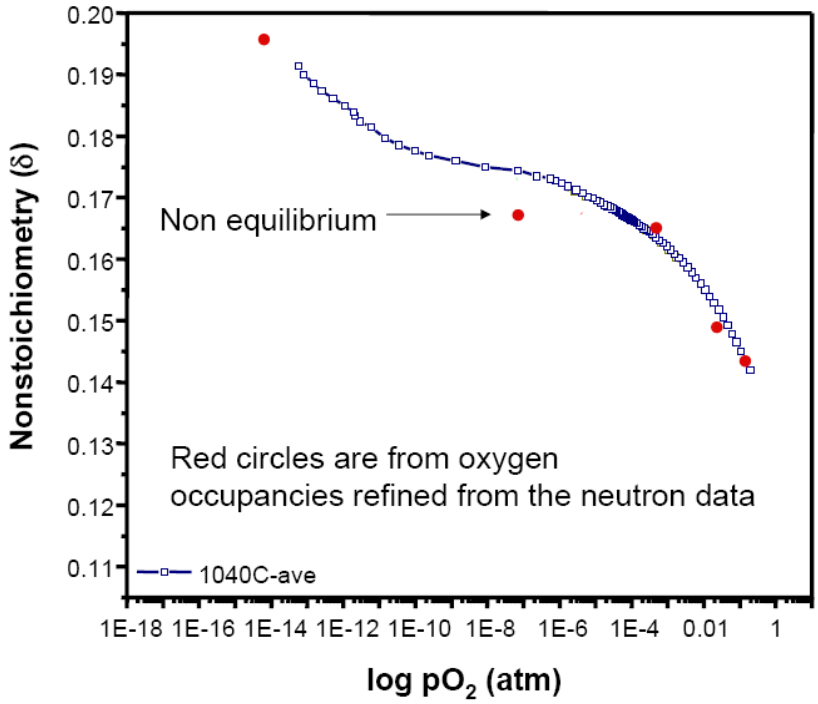

Figure 6 Stoichiometry of $La_{0.2}Sr_{0.8}Fe_{0.55}Ti_{0.45}O_{3-\delta}$ (LSFT) [2]

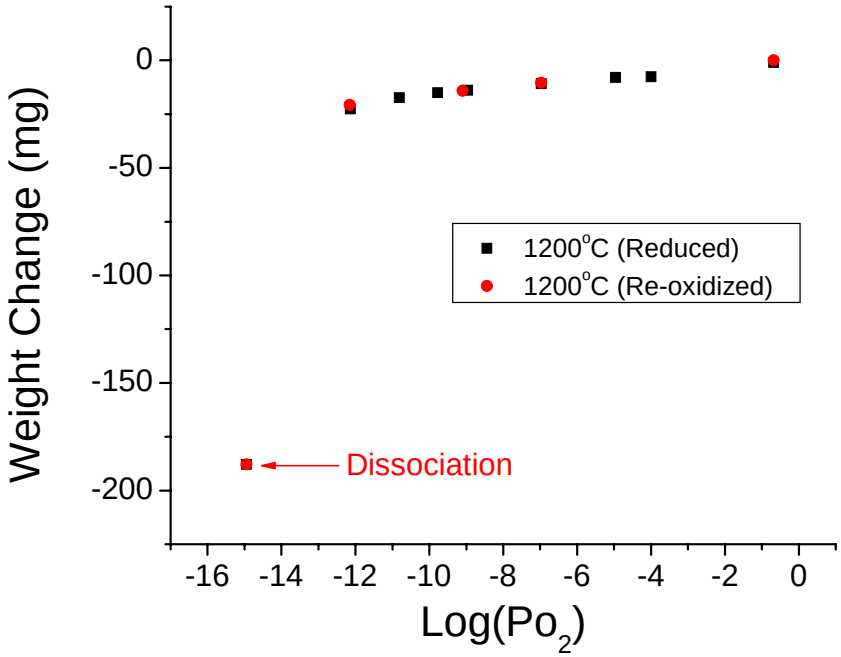

Figure 7 Weight changes of LSFT as a function of oxygen activity at 1200°C

3. Electrical Conductivity and Seebeck Coefficient of LSFT in Air

The electrical conductivity and Seebeck coefficient were measured on dense LSFT (>90% of theoretical density) as a function of temperature and oxygen activity. The electrical conductivity in air was about 2 S/cm at 200°C and reached to the maximum value of 13 S/cm at 500°C and then decreased to 4 S/cm at 1200°C (Figure 8). The Seebeck coefficient is inversely related to the electrical conductivity. It decreased from 30 to 20 μV/K between 200 and 500°C and then increased to about 150 μV/K at 1200°C.

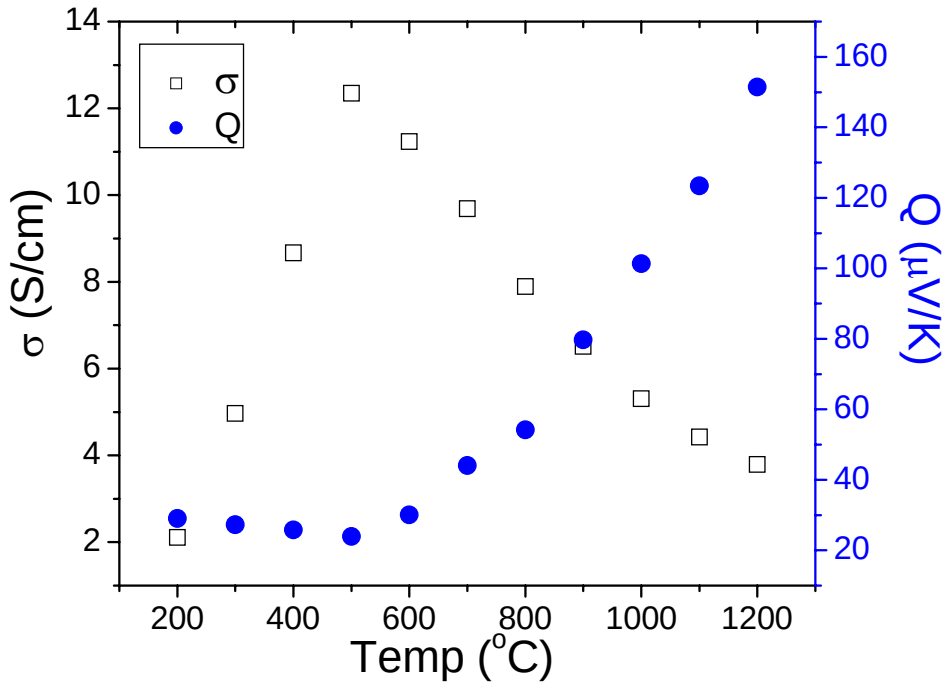

Figure 8 Total conductivity and Seebeck coefficient of LSFT as a function of temperature.

The Seebeck Coefficient and charge carrier concentration are also inversely related through the relationship

$$Q = \pm \frac{k}{e}[\ln(\frac{1-c}{c})] \qquad (1)$$

where Q is the Seebeck Coefficient in μV/K or μV/C, k is Boltzmann's constant, c is the ratio of charge carriers to available conduction sites. Equation (1) was used to evaluate the charge carrier and acceptor dopant concentration. As can be seen in Figure 9, the charge carrier concentration was initially about $8x10^{21}$ at 500°C and then decreased to $2x10^{21}$ at 1200°C as Q increased. Figure 10 shows that the value of the net acceptor dopant concentration as function of temperature. As can be seen, the average value was found to be about 0.35. In $La_{0.2}Sr_{0.8}Fe_{0.55}Ti_{0.45}O_{3-\delta}$ (LSFT), the acceptor ($[Sr'_{La}]$) is

compensated by the donor ($[Ti^{\bullet}_{Fe}]$), thus if the dopants are homogenously distributed in the lattice and are fully ionized, the hole concentration is given by the relation $p = [Sr'_{La}] - [Ti^{\bullet}_{Fe}]$. Thus for the composition used in this study, the net hole concentration should be, p = 0.8-0.45 or 0.35, which agrees with that calculated from the Seebeck measurements. This suggests that both the donors and acceptors were completely ionized and were homogeneously incorporated into the perovskite lattice.

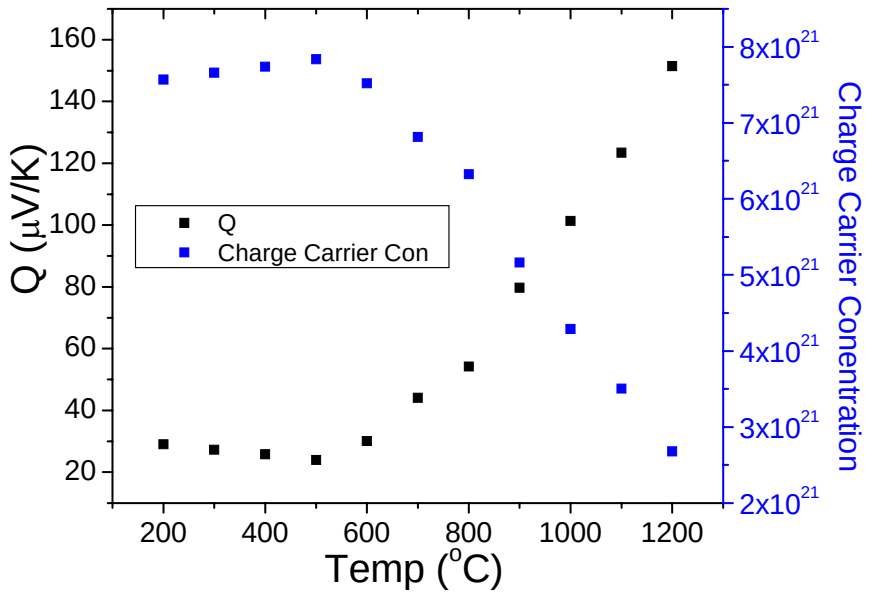

Figure 9 Charge carrier concentration and Seebeck coefficient of LSFT as a function of temperature

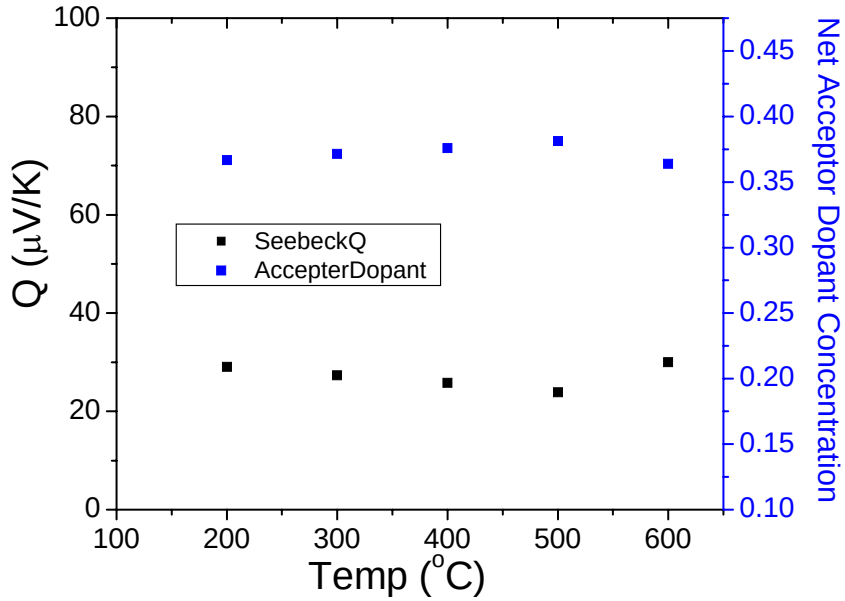

Figure 10 Net acceptor dopant concentration and Seebeck coefficient of LSFT as a function of temperature

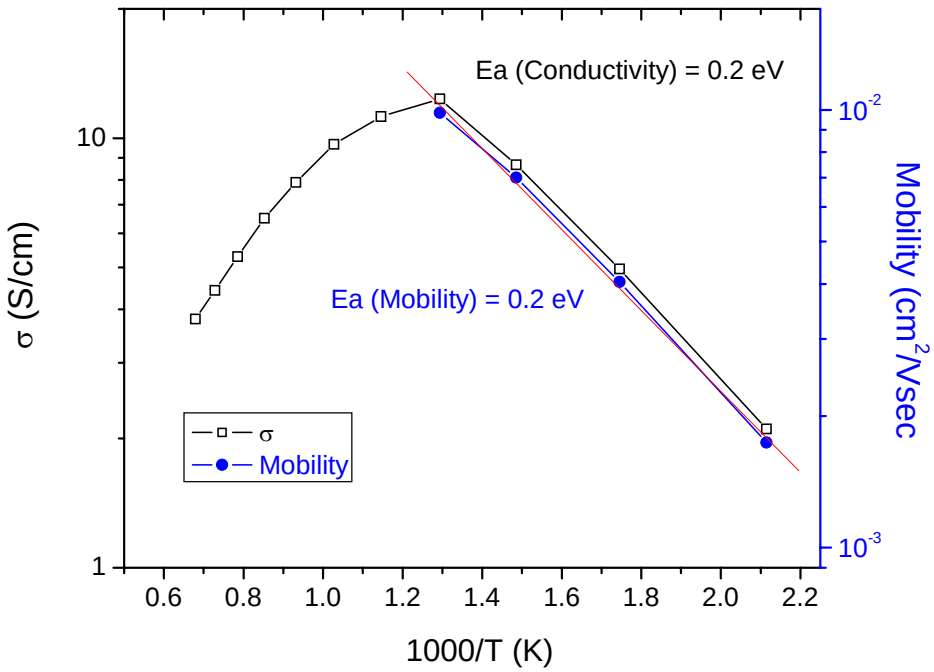

Figure 11 σ vs. 1/T of LSFT and corresponding mobility measured in air as a function of temperature

As shown in Figure 11, the activation energy of conduction for LSFT was about 0.2 eV. The hole mobility was also calculated using the electrical conductivity and carrier concentration data and the results along with the electrical conductivity of the LSFT samples are shown in the Figure 11. The activation energy for the mobility is 0.2 eV which implies that LSFT conducts via the small polaron conduction mechanism.

4. Electrical Conductivity and Seebeck Coefficient as a function of oxygen activity

The *in situ* electrical conductivity and Seebeck coefficient measurements were made on LSFT at 1000 and 1200°C over the oxygen activity range from air to 10^{-15} atm. As can be seen in Figure 12 the LSFT shows a p-type to n-type transition as the oxygen activity from that in air to 10^{-15} atm. The p-type to n-type transition occurred at an oxygen activity of $1x10^{-10}$ at 1000°C and $1x10^{-6}$ at 1200°C. The whole plot including the minimum point (the electrical conductivity at the p-type to n-type transition) in the Figure 12 was shifted to higher oxygen activity range when the temperature was increased from 1000 to 1200°C which is typical of p-type oxides. This shift is related to the fact that the oxygen vacancy concentration is higher at the higher temperature which tends to compensate the p type carriers at higher oxygen activity.

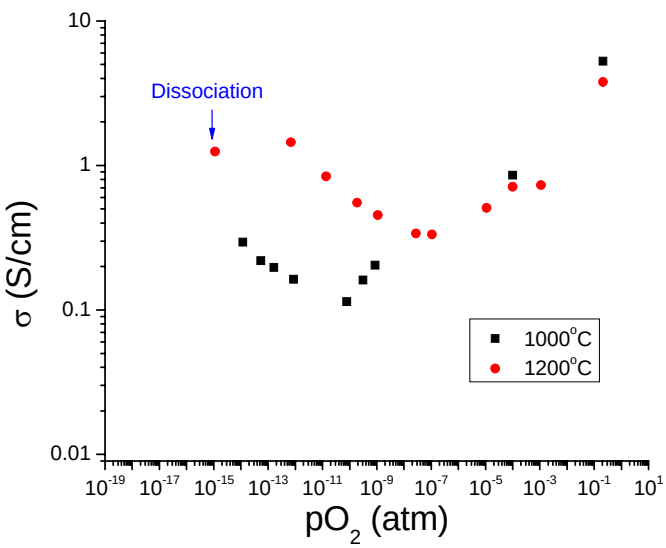

Figure 12 Electrical conductivity as a function of oxygen activity of LSFT at 1000 and 1200°C.

This phenomenon is because in the p type conduction region, $p = [Sr'_{La}] - 2[V^{\bullet\bullet}_{O}]$. Since the concentration of oxygen vacancy, $[V^{\bullet\bullet}_{O}]$, is higher at 1200°C than at 1000°C, the electrical conductivity of LSFT at 1200°C is lower in the p-type regime because the holes which result from the acceptor concentration, $[Sr'_{La}]$, are compensated by the oxygen vacancies. As the oxygen activity continues to be decreased, the n-type conductivity regime is entered when sufficient oxygen vacancies have been generated to totally compensate the acceptors. At this point, the conductivity starts to increase with further decreases in oxygen activity with a negative pressure and exponential temperature dependency. This results in the n-type conductivity at 1200°C being higher than that observed for 1000°C. Further decrease of the oxygen activity below $1x10^{-13}$ atm appeared to cause dissociation or phase changes. The increase of $[V^{\bullet\bullet}_{O}]$ and evidence of dissociation in n-type regime was verified by TGA study shown in Figure 5 and 7. These results agreed with the experimental results from University of Houston (Figure 13) [2].

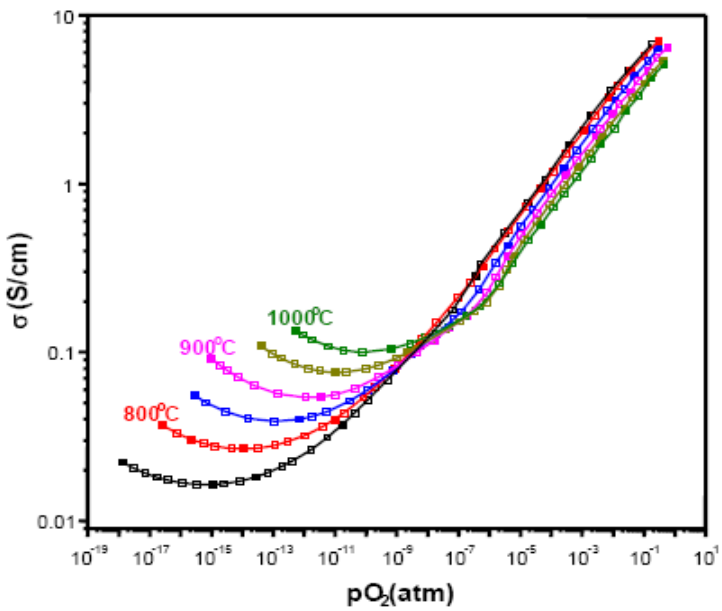

Figure 13 Log σ vs. Po_2 of dense $Sr_{0.9}Ti_{0.6}Fe_{0.4}O_{3-\delta}$ (sintered at 1600°C) at 800°C [2]

Seebeck coefficients were also measured as a function of oxygen activity at 1000 and 1200°C (Figure 14). As can be seen in the Figure 14, the Seebeck coefficient verified that the LSFT has p-type conductivity in high oxygen activity regime and n-type

conductivity in the low oxygen activity regime. The Seebeck coefficient also exhibited that the LSFT has the p-type to n-type transition at about $1x10^{-8}$ and $1x10^{-6}$ atm of oxygen activity at 1000 and 1200°C. However, the electrical conductivity measurement of LSFT exhibited its p-type to n-type transition at about $1x10^{-10}$ and $1x10^{-6}$ atm of oxygen activity at 1000°C at 1200°C. The difference between the two measurements may be due to differences in the carrier mobilities.

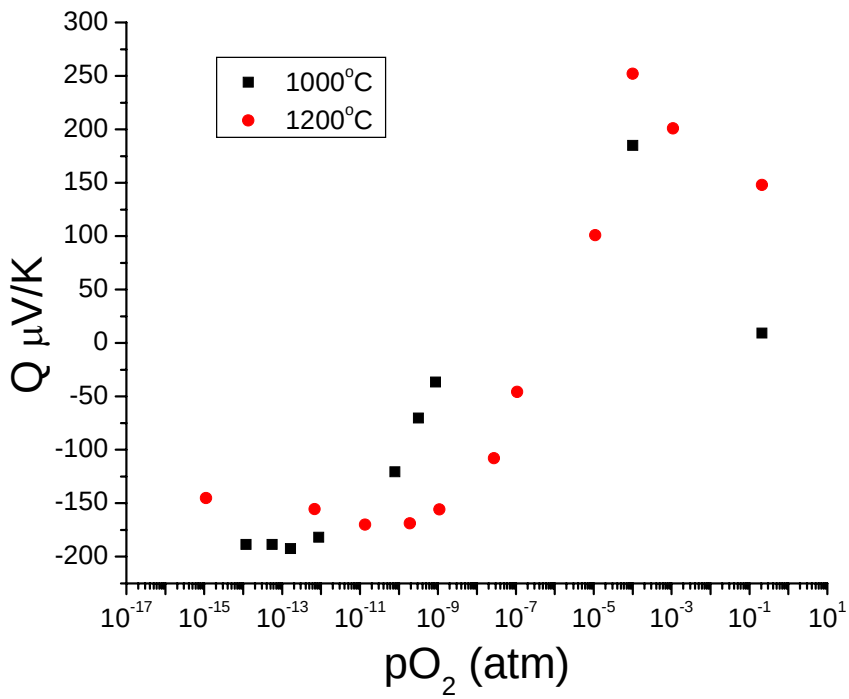

Figure 14 Seebeck coefficient vs. Log Po_2 of ~ 50% dense $La_{0.2}Sr_{0.8}Fe_{0.55}Ti_{0.45}O_{3-\delta}$ (LSFT) at 900°C

Future Studies

1. The optimum composition of LSFT to maximize performance by increasing the concentration of oxygen vacancies and electrical conductivity needs to be established.
2. The temperature and oxygen activity limit for the chemical and mechanical stability of LSFT need to be determined..
3. The relation among the charge carrier concentration, mobility, and net acceptor dopant concentration needs to be evaluated.

Task 2: Determine material mechanical properties under conditions of high temperature and reactive atmosphere

Prof. S. Bandopadhyay and Dr. T. Nithyanantham
University of Alaska Fairbanks, AK 99775

INTRODUCTION

Oxygen ion conducting perovskite-type oxides are very promising materials for potential applications including cathodes for solid oxide fuel cells (SOFCs), membranes for syngas generation, oxygen separation, and the partial oxidation of hydrocarbons [3-6]. The mixed perovskite conductors exhibit not only high ionic conductivity because of the high concentration of oxygen vacancies but also have a high electronic conductivity due to the mixed-valence states. Among various oxides studied, the perovskites (ABO_3) with La, Sr at the A site and B site primarily occupied by Fe are considered to be of commercial interest. These oxides are also observed to exhibit good oxygen permeability with improved stability [7, 8]. However, it has been postulated that all the membrane requirements are not fulfilled by a single phase material [9] and there is a need for a dual phase (composite) membrane. Studies on dual phase composite membranes made of an oxygen ion-conducting oxide and an electron conducting phase have shown much promise with higher oxygen permeability and relatively good chemical and mechanical stability at elevated temperatures [9].

The titanium-substituted perovskites, $SrTi_{1-x}Fe_xO_{3-\delta}$ (STFO) are reported to have a relatively high level of mixed conductivity with an ionic conductivity of, 0.2S cm^{-1} at 1000°C [10-12]. However, their relatively high thermal expansion coefficients (TECs) and poor stability both in highly reducing conditions and increased reactivity with zirconia have limited their use [11-13]. It has been observed that lanthanum substitution on the A-site ($La_{1-x}Sr_xFe_{1-y}Ti_yO_{3-\delta}$), lowers the thermal expansion and enhances the stability [11-13]. The electrical conductivity, oxygen nonstoichiometry (δ) and thermal

and chemical expansion of $La_{0.2}Sr_{0.8}Fe_{0.55}Ti_{0.45}O_{3-\delta}$ (LSFT) has been extensively studied as a function of oxygen partial pressure (pO_2) [8,14]. Likewise, ceria doped solid electrolytes are known for their high oxide ion conduction. The highest level of oxide ion conductivity is characteristic of the solid solutions $Ce_{1-x}M_xO_2$ where M = Gd or Sm, x = 0.10 – 0.20 [15]. At temperatures below 1000 K, $Ce_{0.9}Gd_{0.1}O_{2-\delta}$ (CGO) has been reported to possess a better stability at reduced oxygen pressures than any other related compositions [15].

Development of composite membranes consisting of perovskite type LSFT and fluorite type CGO would be of wise initiative to harvest the advantageous of both the materials. However, for practical applications, the knowledge of the mechanical reliability of the dual phase composite is also very much important. Compatibility of the TEC among constituent phases is an important criterion in developing any ceramic composites. A maximum TEC value of ~12 x 10^{-} K^{-1} and an average TEC value of 9.3 x 10^{-} K^{-1} are reported for the LSFT [14] and a corresponding value of 13.4 ± 1.1 x $10^{-6}K^{-1}$ is reported for CGO [15]. Although, the LSFT and CGO are having almost similar thermal expansion coefficients, they also display a strong dependence of chemical expansion on the oxygen nonstoichiometry at both lower oxygen partial pressure (pO_2) and at high temperatures [14, 17]. The chemical expansion is an isothermal expansion under reducing atmospheres. A liner correlation between thermal expansion and oxygen nonstoichiometry was reported for the LSFT [14] and the expansion due to generation of oxygen ion vacancies was observed at temperatures higher than 600ºC in $N_2/H_2/H_2O$ mixtures for CGO [17]. This chemical expansion of LSFT and CGO are expected to influence the mechanical properties of the dual phase membranes when they are exposed to reducing conditions. In the present work, initial results on the strength and fracture characteristics of the dual phase composite membrane consisting of $La_{0.2}Sr_{0.8}Fe_{0.6}Ti_{0.4}$ (LSFT) oxide and gadolinium doped ceria $Ce_{0.9}Gd_{0.1}$Oxides (CGO) are studied with the intention of understanding the influence of chemical expansion of constituent phases on the fracture behavior in the dual phase composite.

EXPERIMENTAL PROCEDURES

Sintered rectangular bars of $La_{0.2}Sr_{0.8}Fe_{0.6}Ti_{0.4}O_{3-\delta}$ - $Ce_{0.9}Gd_{0.1}$ oxide dual phase composites (LSFT-CGO) were prepared by a proprietary process involved cold isostatic pressing and sintering. The LSFT and CGO (40/60 volume %) powders were mixed and cold isostatically pressed at 20,000 psi prior to the sintering at 1400°C for 4hrs. The as-sintered bars were characterized using SEM, XRD and thermogravimetry. Microstructure analysis of the as-sintered (as-received) membrane was done on samples sectioned, ground and polished to 1μm finish using successive grades of SiC paper and finally with a diamond paste. The polished samples were thermally etched at 1350ºC for 30 min in air. At 1000ºC, a δ value closer to 0.175 is reported for LSFT when the partial pressure of oxygen is reduced to 10^{-4} {UHP grade N_2}[8]. Therefore, several sectioned membranes were heat treated at 1000ºC in N_2 for 1 hr to alter the oxygen nonstoichiometry (δ) of the LSFT. A flow of N_2 (200 ml/min) was maintained through out the heat-treatment including heating and cooling to maximize the reduction and prevent any re-oxidation during cooling. Some of the membranes were heat treated at 1000°C in air for 1 hr with the similar heating rates for comparative studies. The 'heat treated' samples also characterized using XRD, thermogravimetry and SEM. The hardness and fracture toughness of the as-sintered and heat treated samples were estimated using Vicker's indentation method. A load of up to 10N was applied for 10 seconds and the fracture toughness of the membranes was calculated using the equations of Niihara et al. [12]. The indentation crack propagation was studied using SEM and optical microscopy for identifying any possible influence in the fracture behavior due to the change in the δ.

Flexural strength test specimens of dimensions (3x4x48 mm) were cut from the as-sintered bars and tested *in-situ* in an autoclave mounted on a servo-electric loading frame. Loading was done in an in-house designed 4-point flexure with an outer span of 38.1 mm and inner span of 19.05 mm (ASTM-B). The specimens were ground and polished to 3 μm finish using successive grades of SiC paper and finally with a diamond paste and the edges barreled. In addition, the tensile side was polished using diamond paste of 1μm prior to the test. Strength tests were carried out at room temperature and at

1000°C in slightly reducing atmosphere (N_2) atmosphere. In the N_2 atmosphere, the specimen was loaded in the fixture and heated to 1000°C for 1 hour prior to application of any load while the N_2 was purged continuously. The furnace power was completely shut off after the fracture of the specimen and allowed to cool. The flexural strength was calculated using the simple beam formula,

$$\text{Fracture strength } (\sigma_f), \text{ MPa} = \left(\frac{3PL}{4BW^2} \right) \quad \text{---- (1)}$$

Where P = Fracture Load (N); Outer Span (here 3.81 cm); B= thickness and W= width of the beam respectively. The post fracture dual phase membranes were characterized by thermogravimetric analysis, X-ray diffraction and scanning electron microscopy to understand the fracture behavior.

RESULTS AND DISCUSSION

Characterization

The percolation of both phases is clearly observed in the SEM micrographs of the 'as-received' membrane, which are shown in Fig 15. The CGO grains are brighter and the LSFT grains are darker in the micrographs. The LSFT and CGO grains are uniformly distributed and no micro cracks and any other flaws caused by the thermal expansion mismatch of the phases.

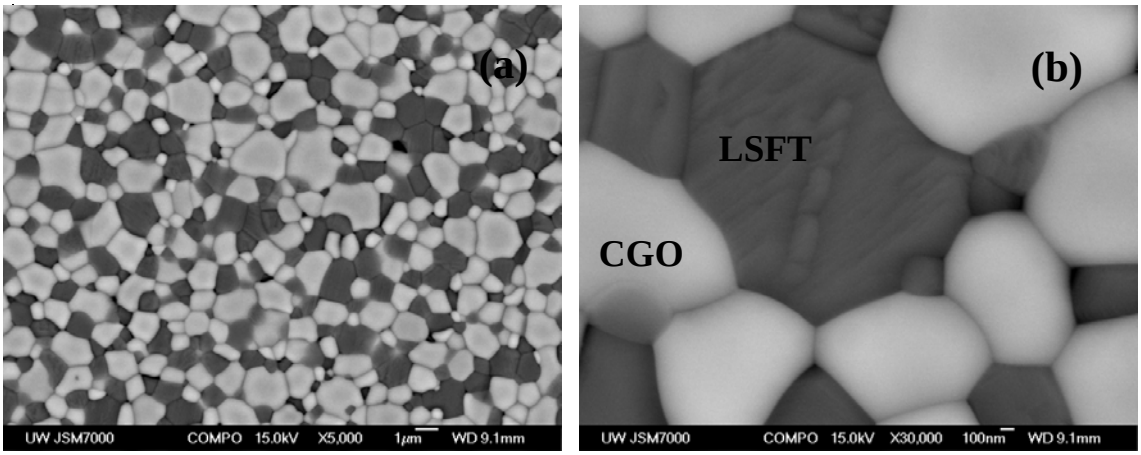

Figure 15. Back scattered SEM micrographs of the 'as-received' LSFT-CGO membranes. The dark phase is LSFT and the bright phase is CGO. Percolation of the two-phases is clearly observed in (a) and no micro cracks and any other flaws caused by the thermal expansion mismatch are visible at the grain boundaries (b).

The X-ray diffraction pattern of the 'as-received' membrane shown in Figure 16 also confirms the co-existence of LSFT and CGO phases. Slow scan X-ray data did not reveal any secondary phases formed due to interaction between the two phases. Figure 17 shows TGA curves of the as-received membrane in air and N_2 environment. The weight loss starts at around 300ºC and the maximum weight loss of 0.22% was observed at 1000ºC in air. About a 60% of this total weight loss is reversible due to the loss of oxygen from the LSFT and CGO. Similar weight loss due to the oxygen loss was reported for LSFT by Zhou *et al* [18]. The slightly reducing N_2 environment cause a total weight loss of 0.62% at 1000°C in which 93% is due to oxygen loss which is irreversible in the N_2 atmosphere (log Po_2 = -4).

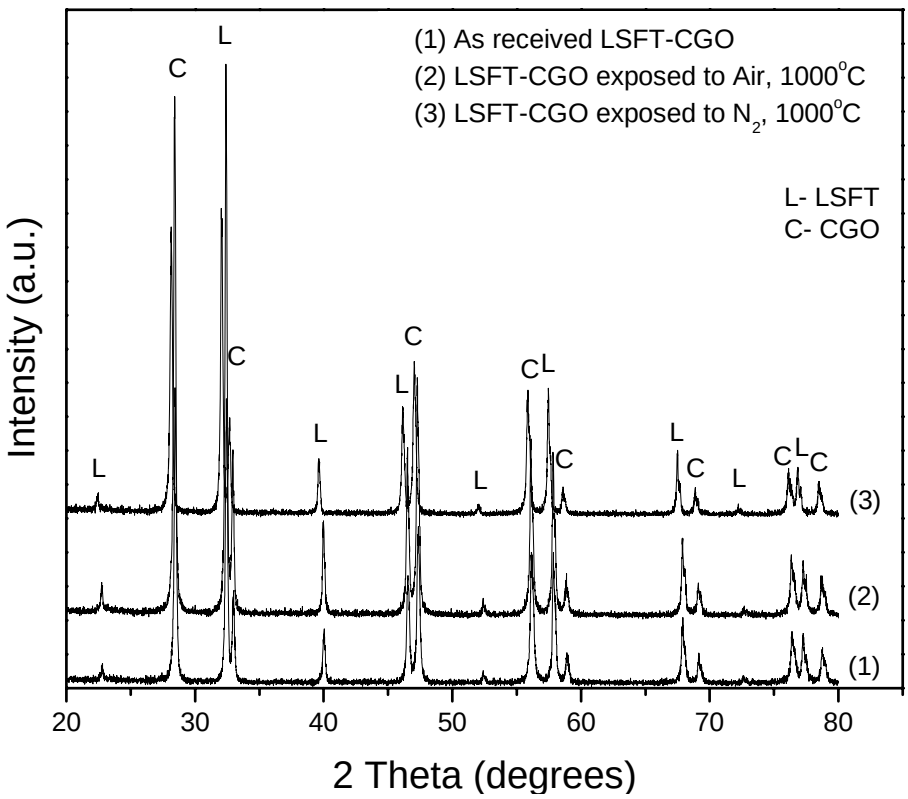

Figure 16. The XRD patterns for LSFT-CGO membranes.

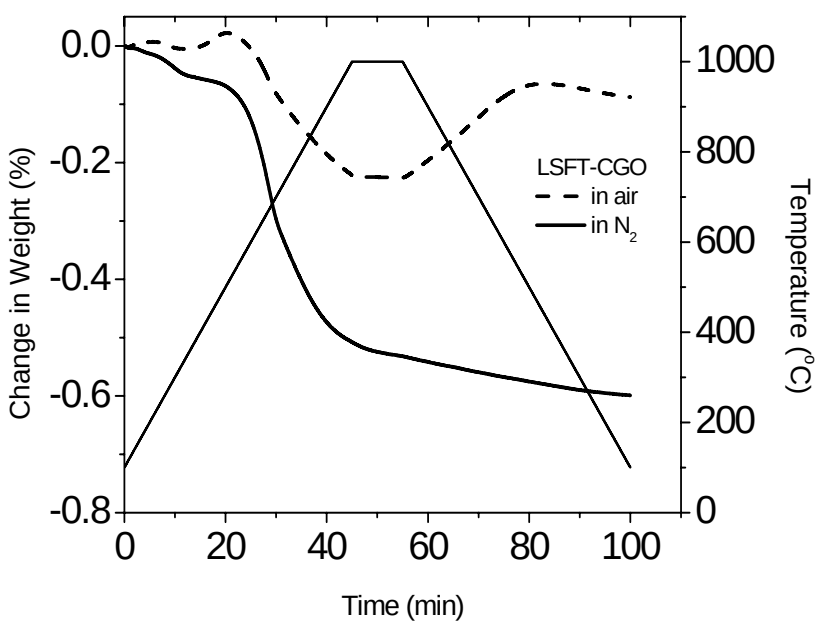

Figure 17. Change in weight for LSFT-CGO in air and N_2 environment.

MECHANICAL PROPERTIES

Hardness and fracture toughness

The hardness values and fracture toughness of the membrane were measured as a function of the load and the results of the 'as-received' and heat-treated are presented in Fig 18.

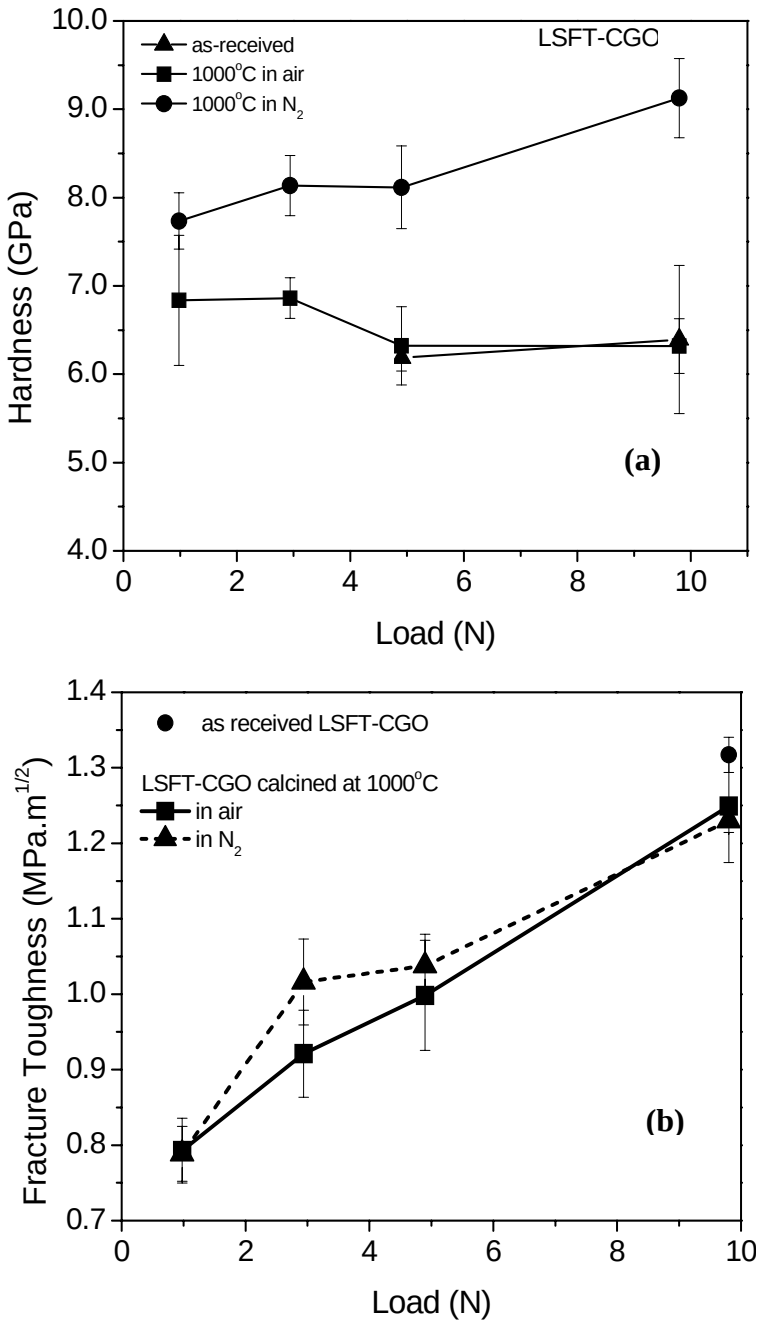

Figure 18. Dependence of the hardness (a) and Fracture toughness (b) of dual phase membranes on indentation load

The hardness value of the ‘as-received’ membrane increases till 4.9 N and remains the same at the higher load. After heat treatment in air, the hardness of the membrane has increased at the lower indentation load and remains mostly stable for all the other loads. From Fig 18a, it is evident that the hardness of the dual phase membrane is significantly affected by the atmosphere in which it was heat treated. At a given load, the hardness of the N_2 treated membrane is significantly higher than air-treated samples. This indicates probable effects of reducing atmosphere on the structural behavior of the membrane at the elevated temperatures. However, the fracture toughness values are found to be increasing with increasing load irrespective of the environment it was heat-treated. For the ‘as-received’ membranes the fracture toughness value was estimated to be as 1.32 $MPa.m^{1/2}$ at 9.8 N.

The heat-treated membranes clearly showed stable initial crack growth, in that the fracture toughness increases with increasing indentation load. This kind of behavior can be interpreted as a possible rising R-curve behavior. The effect of environment on 'L/a' as a function of applied indentation load is plotted in Fig 19 where L is the crack length and the 'a' is the half of the indentation diagonal. The increasing 'L/a' value also implies the presence of an active toughening mechanism, which resists the growing crack. In general, the R-curve like behavior is indicative of possible toughening mechanisms, such as crack-deflection, crack-bridging, crack-branching, and frictional interlocking of grains that are active in the non-transforming ceramics. These toughening mechanisms "shield" the crack tip from the applied loads. The 'L/a' value for the membrane heat treated at N_2 was significantly higher at the higher loads. This higher 'L/a' values can be related to higher hardness values of the membranes treated at N_2 or some additional toughening that resists the crack growth or both.

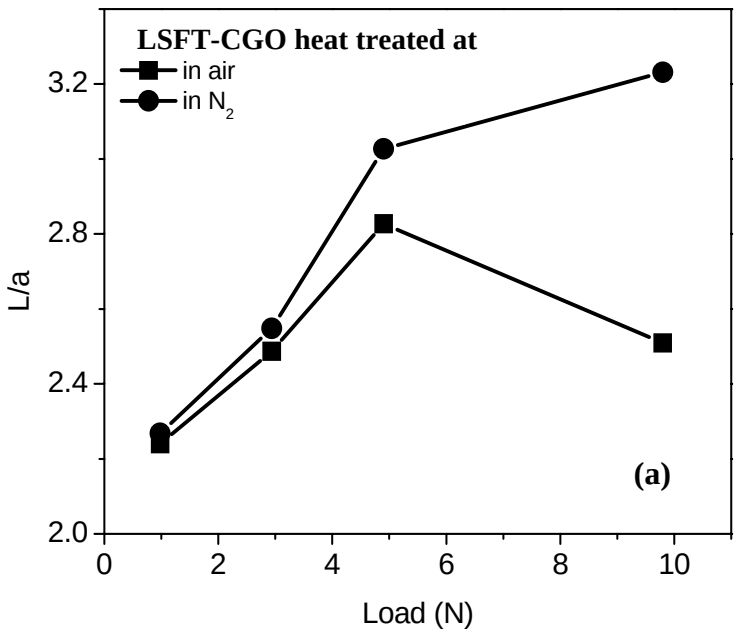

Figure 19. The crack propagation behavior of dual phase membrane. The dependence of L/a on indentation load indicates the presence of some toughening mechanisms in the membrane.

The XRD analyses reveals that the heat treatment of the membrane at 1000°C in air and N_2 atmosphere resulted in no phase changes or decomposition of the membrane which invalidate the involvement of any second phases or decomposition product in the mechanical properties of the membrane.

FLEXURAL STRENGTH AND FRACTOGRAPHY

The effect of temperature and environment on the flexural strength of the dual phase membrane is shown in Fig 20. The flexural strength was evaluated to be 104 MPa and 51.2 MPa for dual phase membranes in room temperature (in air) and at 1000°C in N_2 respectively.

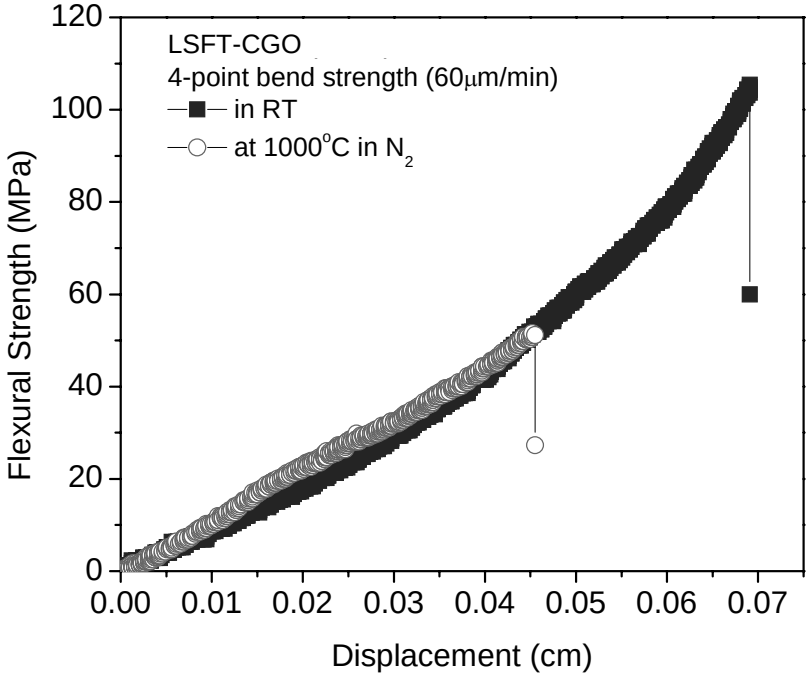

Figure 20. Effect of temperature and environment on the flexural strength of the dual phase membrane

The SEM micrographs of the fracture surfaces show a significant difference in the mode of fracture (Fig 21) between the membranes fractured in air and at 1000°C in N_2. The membranes fractured at room temperature showed mostly transgranular fracture. However, the membranes fractured at 1000°C in N_2 environment showed mostly intergranular fracture (Fig 21c and 21d), which suggests a crack path along the boundaries. The fracture-path transition from transgranular to intergranular can be associated to probable tensile stresses at the grain boundaries that promote the interfacial debonding at the wake of advancing crack tip. The transgranular fracture behavior of the 'as-received' membranes neglects the presence of any residual stress caused by the thermal expansion mismatch of the constituent phases. Hence, the fracture mode transition can be correlated largely to the thermally induced chemical expansion of the LSFT and CGO.

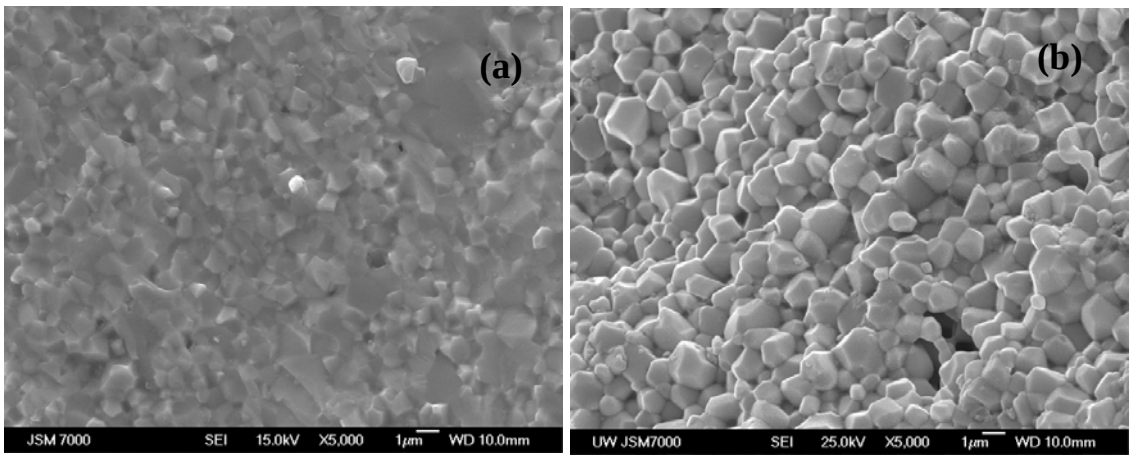

Figure 21. SEM micrographs of fracture surfaces at room temperature (a) and at 1000°C in N_2 (b). Fracture was mainly transgranular at the room temperature and intergranular at 1000°C in N_2 atmosphere.

The thermal and chemical expansion properties of LSFT at $800 \leq T \leq 1200$°C and at $\sim 1 \times 10^{-15} \leq pO_2 \leq 0.21$ atm were reported by Park and Jacobson [14] which established a liner correlation between thermal expansion and oxygen nonstoichiometry at 800°C. At higher temperatures, the chemical expansion showed a pronounced non linear dependence on stoichiometry. Similarly, a chemical expansion behavior of CGO is also reported above 600°C in the reducing conditions. In order to confirm the oxygen loss of the membrane during the strength test at N_2 atmosphere, a post fracture thermal analysis was carried out on the fractured membrane. The TGA curve is shown in Figure 22. The weight gain of the membrane during TGA in air not only indicates non-stoichiometry of the membrane during the strength test but also imply that the membrane remain oxygen deficient even after the strength test.

An indentation was made on the membrane fractured at 1000°C in N_2 and the crack path was examined using SEM with the purpose of understanding the choice of crack path as well as the contribution of constituent phases for any possible toughening mechanisms like crack-bridging and frictional interlocking of grains. A representative crack path is shown in Figure 23. The crack propagation was mostly along the boundaries of the LSFT (darker grains), irrespective of the angle at which it encounter the LSFT grain. Hardly any LSFT grain was cleaved during its course and is consistent with

expected toughening in the crack wake via crack bridging from interlocking grains that act to shield the crack tip from the applied far-field load. It can be speculated that a possible stress gradient at the grain boundaries caused by the volume expansion of the LSFT unit cells could lead to changes in the fracture mode from transgranular to intergranular that promotes the grain bridging and frictional interlocking of grains. Accordingly, a rising R-curve like behavior would be anticipated and lead to an increase in fracture strength. However, such concomitant increase of the crack growth resistance and fracture strength is seldom confirmed by experimental measurements in ceramic materials. In this study, even though the reducing atmosphere at elevated temperature has changed the crack path and promoted more toughening, it is clear that it has reduced the strength of the membranes significantly.

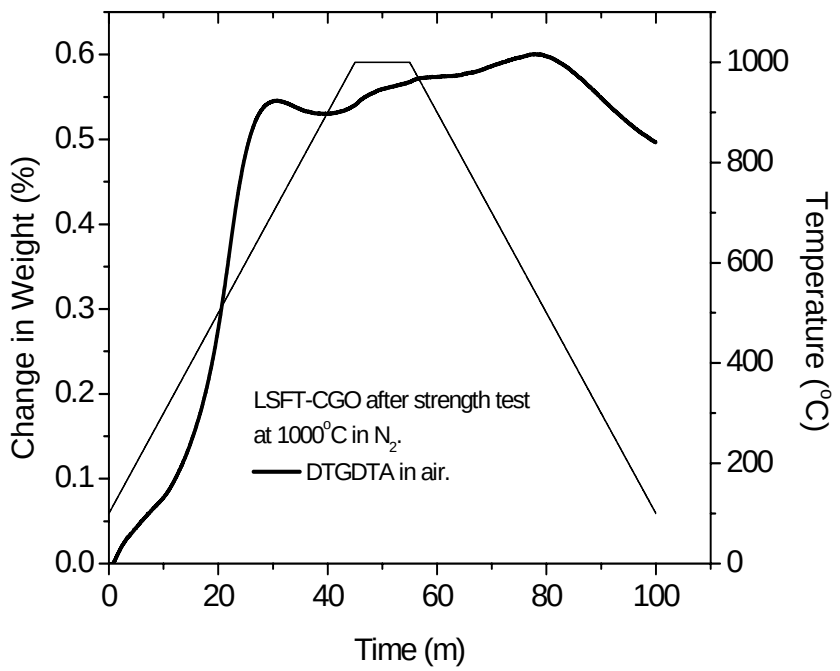

Figure 22. Change in weight of the LSFT-CGO in air. The weight gain of the membrane during TGA in air not only indicates non-stoichiometry of the membrane during the strength test but also implies that the membrane remain oxygen deficient even after the strength test.

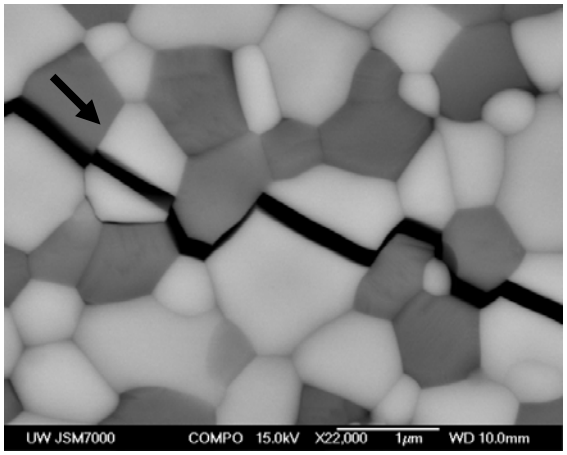

Figure 23. Back scattering electron micrograph of a crack path. The arrow mark shows the direction of crack propagation. The darker grains are LSFT and brighter grains are CGO. Note the crack prefers the boundaries of LSFT and cleaves the CGO on its course.

The exact contribution of the chemical expansion induced stress on the failure of the membranes is yet to be fully understood. A systematic investigation of the influence of oxygen partial pressure on the mechanical properties can help in understanding the correlation between the non-stoichiometry and the strength. Also, high temperature modulus studies of these membranes at the reducing environments also will be of useful.

Plans for the Next Quarter.

1. Effect of reducing atmosphere on thermal and chemical expansion will be studied for the dual phase membranes
2. The hardness and fracture toughness of the as-received membranes and heat-treated membranes will be evaluated.
3. Detailed thermogravimetric analysis and X-ray diffraction studies for all three compositions to understand the chemical expansion of the membranes.

Task. 3: Measurement of Surface Activation/Reaction Rates in Ion Transport Membranes using Isotope Tracer and Transient Kinetic Techniques

A. J. Jacobson, University of Houston, C.A. Mims, University of Toronto

INTRODUCTION

Mixed ionic electronic conductors (MIECs) with the ABO_3 perovskite or related structures have been widely studied because of their practical applications in ion-transport membranes, pressure-driven oxygen generators, partial oxidation reactors, and as electrodes for solid oxide fuel cells (SOFCs) [19] A number of materials problems remain outstanding for the application of ion transport membrane reactors in the high oxygen partial pressure gradients found, for example, in *syn gas* generation by partial oxidation of methane. The membrane composition must simultaneously provide the necessary oxygen flux and have stability over a wide pO_2 range and appropriate mechanical properties. Our previous findings from isotopic transients show that surface reaction rates on both sides of the membrane are significant kinetic barriers to membrane performance and that the oxidation reactions on the "fuel" side of a syngas membrane can show bistable behavior indicative of a strong coupling between the surface reactivity and the surface composition and oxidation state.

The $La_{1-x}Sr_xFeO_{3-x}$ (LSFO) series has high mixed conductivity and better stability than the $La_{1-x}Sr_xCoO_{3-x}$ (LSCO) series but still exhibits limited stability in low-pO_2 environments. Additional substitution on the B-site by metal ions that are more difficult to reduce solves some of these problems but issues remain concerning both kinetic and thermodynamic stability and the effects of composition changes that result from partial decomposition or surface segregation on the membrane surface catalytic properties.

In our studies of membrane materials, we have investigated the pO_2 and temperature dependence of the conductivity, non-stoichiometry and thermal-expansion behavior of two specific compositions, $La_{0.2}Sr_{0.8}Fe_{0.8}Cr_{0.2}O_{3-x}$ and $La_{0.2}Sr_{0.8}Fe_{0.55}Ti_{0.45}O_{3-x}$, by using

electrochemical cells and dilatometry [20-23]. Additional measurements on the simpler composition, $La_{0.5}Sr_{0.5}FeO_{3-x}$ have been made for comparison [24]. These and other recent studies of ferrites with the perovskite structure show anomalous behavior at low oxygen partial pressures ($<10^{-5}$ atm). Temporary nano-phase segregation behavior involving cation ordering is thought play a role in this bulk behavior. Such behavior is also consistent with the unusual surface reactivity findings. During this reporting period, we have reviewed the data on $La_{0.2}Sr_{0.8}Fe_{0.8}Cr_{0.2}O_{3-x}$ with a view to obtaining additional insight into the properties at intermediate pO_2.

EXPERIMENTAL

The experimental methods have been described in previous reports.

RESULTS

a. Electrical Conductivity

The pO_2 dependence of electrical conductivities (σ S cm^{-1}) at 752, 802, 854, 902, 942, 985, 1024, and 1055°C measured with increasing oxygen partial pressure after the cell Had been initially pumped out are shown in Fig. 24.

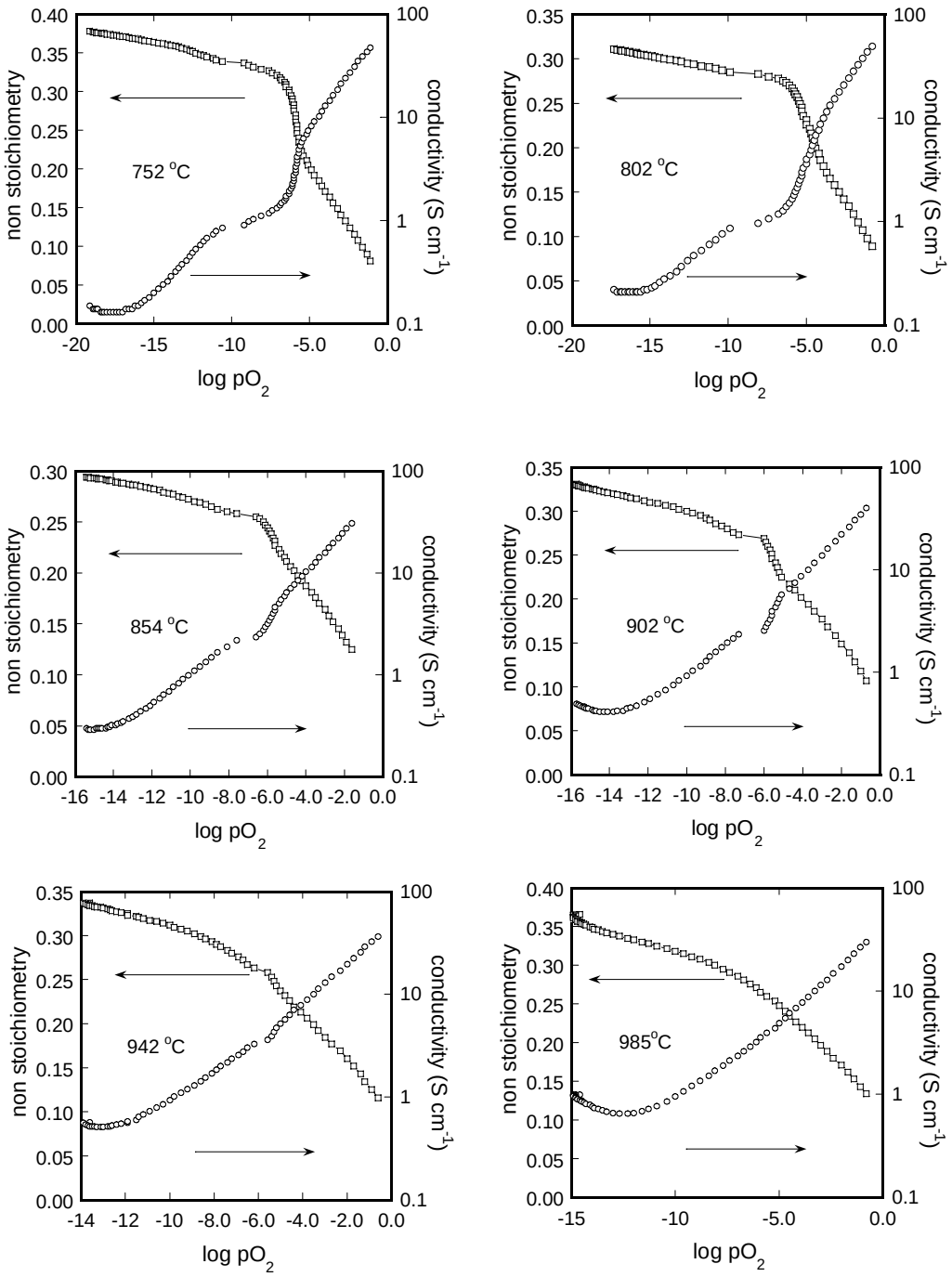

Fig. 24 pO_2 dependence of electrical conductivities at 752, 802, 854, 902, 942, 985, 1024, and 1055°C.

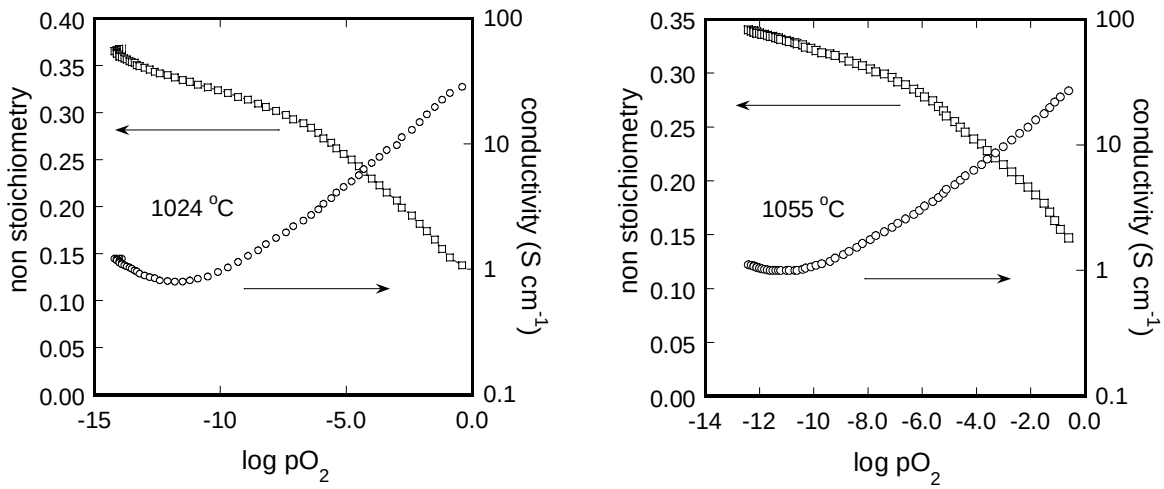

Fig. 24 (cont.) pO_2 dependence of electrical conductivities at 752, 802, 854, 902, 942, 985, 1024, and 1055°C.

When the temperature (T) increased, σ decreased in the higher pO_2 region. The slope of the isotherms is dependent on pO_2, and is ~ 1/5 almost irrespective of T in the p-type region, $pO_2 = 10^{-5} \sim 10^{-1}$ atm (Fig. 25). For noninteracting and dilute defects, σ is proportional to $(pO_2)^{1/4}$, assuming constant mobility. Since 80 % of the A site is doped with Sr, high oxygen deficiency is observed at elevated T and hence defect interactions and association are expected, leading to lower values of the exponent.

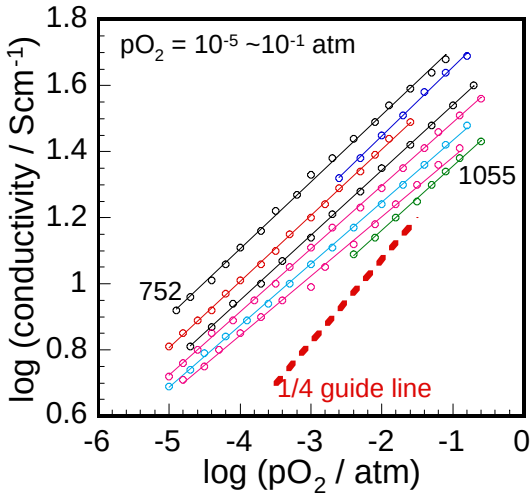

Fig. 25. pO_2 dependence of electrical conductivities in the $pO_2 = 10^{-5} \sim 10^{-1}$ atm

In the pO_2 range between the plateau and the minimum value of σ in the isotherms shown in Fig. 25, the electrical conductivity values are nearly independent of temperature, for example, at $pO_2 = 10^{-10}$ atm the conductivity varies from 0.8 to 1.1 S/cm. The total conductivity (σ_t) is approximately the sum of the electron hole conductivity (σ_h) and the ionic conductivity (σ_i) in this region. Since the values of σ_h and σ_i are comparable in this pO_2 range, a $\sigma \propto (pO_2)^{1/4}$ dependence is not expected. The weak temperature dependence arises because of the opposite temperature dependences of σ_h and σ_i. Thus the decrease in σ_h at higher T is compensated by a higher σ_i.

p-n Transition Behavior and Ionic Conduction

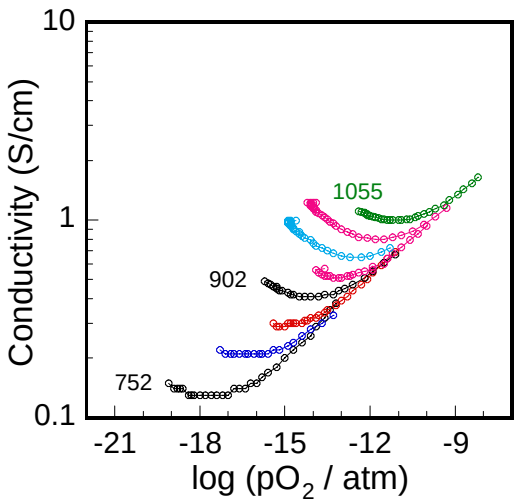

Fig. 26 The temperature dependence of p-n transition behavior

The pO_2 conductivity isotherms are shown in the vicinity of the p-n transition region in Fig. 27. The pO_2 at which the minimum occurs increases with increasing temperature as expected. The p-n transitions of LSCrF occur at pO_2 (atm) = 2.36×10^{-18} at 752°C, 3.65×10^{-17} at 802°C, 6.99×10^{-16} at 854°C, 8.67×10^{-15} at 902°C, 7.41×10^{-14} at 942°C, 2.20×10^{-13} at 985°C, 1.67×10^{-12} at 1024°C, and 6.80×10^{-12} at 1055°C.

At the pO_2 values corresponding to the minimum conductivities (σ_{min}), the ionic transference numbers approach unity and the oxygen vacancy concentrations are independent of temperature. Thus, E_a is mainly due to the ionic mobility term in the conductivity. Assuming that $\sigma_{min}T = A exp(-E_a/RT)$, then a plot of log ($\sigma_{min}$T) vs.1000/T, gives an activation energy of 0.86 eV for ionic conduction. This value of E_a is for the vacancy

ordered-phase, since the values of ionic conductivity were determined in the lower pO_2 region.

Stoichiometry

The relative stoichiometry data measured also from low to high oxygen partial pressure are also shown in Fig.24. The absence of any change in the stoichiometry in the range of oxygen partial pressures corresponding to the plateau in the conductivity data also indicate non equilibrium behavior. The sharp change in stoichiometry at nearly constant pO_2 indicates two phase behavior.

Phase Transition

The plateau region observed in the pO_2 variation of the conductivity and stoichiometry suggests that a two-phase region exists in the temperature range between 752 and 942 °C (Fig. 24.). At high vacancy concentrations and lower temperatures perovskite oxides often phase separate and form vacancy ordered phases to reduce coulombic repulsion among defects.

The general shape of the data suggests, however, that equilibrium is not achieved in this region. Specifically, if a well-defined two-phase region exists then the conductivity should change discontinuously at the pO_2 value at which the two phases are in equilibrium. The magnitude of the discontinuity will depend on the difference in total conductivity between the two phases. The ionic conductivity is directly affected by the vacancy ordering and the electronic conductivity depends on the consequent changes in the electronic structure. The total effect on the conductivity is not easy to predict but general, we might expect the difference to be small since the two phases have the same composition. We note that the change is reported to be small in $SrFeO_{3-\delta}$. The observed behavior can be interpreted as follows. At a given temperature, on increasing pO_2, the conductivity increases from the minimum, through a p-type region, until the plateau is reached. The conductivity then remains constant until a large enough excess oxygen pressure (over-potential) is applied to drive the phase transition. As the phase transition occurs, the conductivity increases until the high-pressure equilibrium line is reached. The kinetics of phase separations between ordered and disordered systems are known to be slow in perovskite oxides as discussed in for $SrFe_{0.2}Co_{0.8}O_{3-x}$. The size of the plateau

region decreases with increasing temperature both because the rate of the phase separation increases and also because the width of the two phase region decreases. By 985 ºC, the plateau region is no longer apparent although a change in slope remains.

In Fig. 27, we show conductivity data at two temperatures measured in the opposite direction, namely from high to low pO_2. Measurements made in this direction show no plateau region at intermediate pO_2 values but only a change in slope. The data at both high and low partial pressures agree with the measurements made in the reverse direction (note that in each case the two sets of data are offset for clarity). Apparently the phase separation is faster from the high-pressure side but whether this is an intrinsic phenomenon or related to mass transfer effects is not yet known.

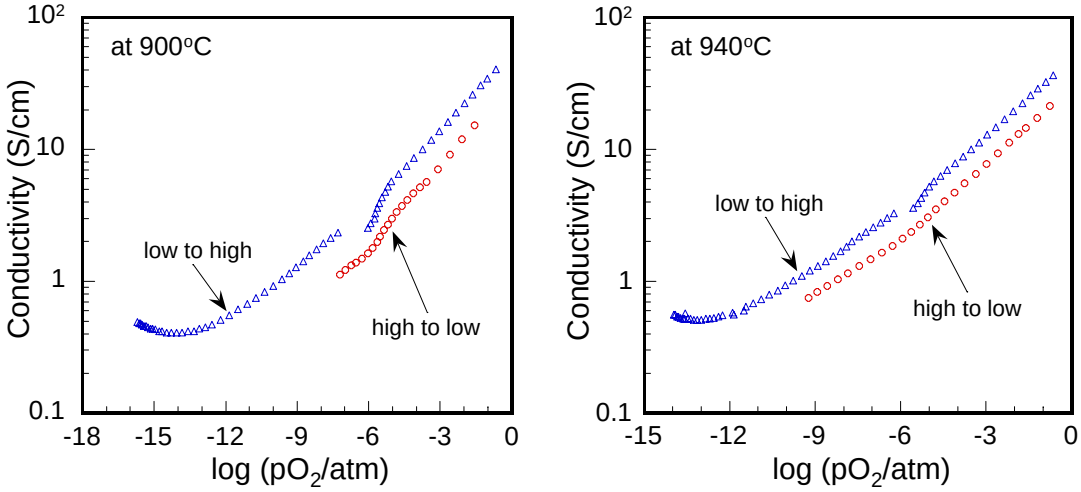

Fig. 27. Comparison of conductivity isotherms according to the direction: "high to low pO_2" run and "low to high pO_2" run. For clarity, "high to low pO_2" runs are offset.

Plans for the Next Quarter.

We plan to continue analysis of additional conductivity and stoichiometry data for LSFCR. This analysis will then be combined with the IEDP and transient membrane reactor data.

CONCLUSIONS

LSFT not only exhibits p-type in the high oxygen activity regime, but also has an n-type in the reducing atmosphere. Higher concentrations of oxygen vacancies in the low oxygen activity regime may improve the performance of LSFT as an OTM. The hole concentration is related to the difference in the acceptor and donor concentration by the relation $p = [Sr'_{La}] - [Ti^{\bullet}_{Fe}]$. The chemical formulation predicts that the hole concentration is, p = 0.8-0.45 or 0.35. Experimental measurements indicated that p is about ~ 0.35. The activation energy of conduction is 0.2 eV which implies that the LSCF conducts via the small polaron conduction mechanism.

The dual phase membranes have been evaluated for structural properties. An increasing crack growth resistance was observed for the membranes heat-treated at 1000°C in air and N_2 with increasing crack length. The flexural strength was evaluated to be 104 MPa and 51.2 MPa for dual phase membranes in room temperature (in air) and at 1000°C in N_2 respectively. The oxygen deficiency in LSFT caused by the N_2 atmosphere at 1000°C is thought to promote intergranular debonding during crack propagation and observed transgranular fracture. Further studies can elucidate on the role of chemical expansion on mechanical properties of dual phase membranes.

The data for the conductivity and stoichiometry data indicate the appearance of a phase transition in LSCRF. We have reviewed the electrical conductivity data and stoichiometry data for $La_{0.2}Sr_{0.8}Cr_{0.2}Fe_{0.8}O_{3-\delta}$ some of which was reported previously. Electrical conductivity data for $La_{0.2}Sr_{0.8}Cr_{0.2}Fe_{0.8}O_{3-\delta}$ (LSCrF) were obtained in the temperature range, 752 ~ 1055 °C and in the pO_2 range, 10^{-18} ~ 0.5 atm. The slope of the plot of log σ vs. log pO_2 is ~1/5 in the p-type region, $pO_2 = 10^{-5} \sim 10^{-1}$ atm. The pO_2 at which the p-n transition is observed increases with increasing temperature. The activation energy for ionic conduction was estimated to be 0.86 eV from an Arrhenius plot of the minimum conductivity vs. reciprocal temperature. At temperatures below 940°C, a plateau in the conductivity isotherm suggests the presence of a two-phase region. Most likely, phase separation occurs to form a mixture of a perovskite phase and an oxygen vacancy ordered phase related to brownmillerite. Non equilibrium effects are observed but unlike those in LSFTO, they become less apparent with increasing temperature.

LIST OF ACRONYMS AND ABBREVIATIONS

CGO	Cerium gadolinium oxide
GDC	Gadolinia doped ceria
IEDP	Isotope exchange –depth profiling
PEG,PEO	Polyethylene glycol, polyethylene oxide
SEM-EDX	Scanning Electron Microscopy–Energy Dispersed X-ray analysis
ToFSIMS	Time of Flight Secondary Ion Mass Spectroscopy
YSZ	Yttria stabilized zirconia
XRD	X-ray diffraction

REFERENCES

UMR

1. D.P. Fagg et al.,"Stability and mixed ionic-electronic conductivity of (Sr,La)(Ti,Fe)$O_{3-\delta}$ perovskites", *Solid State Ionics*, 156 (2003) 45-57

2. A J. Jacobson and C. A. Mims.,"Transport properties and phase stability of mixed conducting oxide membranes", Oxygen Transport Ceramic Membrane Annual Project Review at University of Houston, December 11, 2006

UAF

3. H. J. M. Bouwmeester and A. J. Burgraaf, ''Dense Ceramic Membranes for Oxygen Separation,'' in The CRC Handbook of Solid State Electrochemistry, Edited by P. J. Gellings, and H. J. M. Bouwmeester. CRC Press Inc., Boca Raton, 481–553 (1997).

4. A. Atkinson and A. Selcuk, ''Mechanical Behaviour of Ceramic Oxygen Ion-Conducting Membranes,'' *Solid State Ionics,* **134**, 59–66 (2000).

5. P. V. Hendriksen, P. H. Larsen, M. Mogensen, F. W. Poulsen, and K. Wiik, ''Prospects and Problems ofDense Oxygen PermeableMembranes,'' *Catal. Today*, **56,** 283–95 (2000).

6. V. V. Kharton, E. N. Naumovich, and A. V. Nikolaev, ''Materials of High-Temperature Electrochemical Oxygen Membranes,'' *J. Mater. Sci.*, **111**, 149–57 (1996).

7. D.P. Fagg, V.V.Kaharton, J.R. Frade, and A.A.L. Ferreira, "Stability and Mixed ionic-electronic Conductivity of (Sr,La)(Ti,Fe)$O_{3-\delta}$ Perovskites" Solid *State Ionics***,** **156**, 45-57 (2003).

8. C.Y. Park and A.J. Jacobson, " Electrical Conductivity and Oxygen Nonstoichiometry of $La_{0.2}Sr_{0.8}Fe_{0.55}Ti_{0.45}O_{3-\delta,}$ " *J. Electochem. Soc.,* **152,** J65-J73 (2005)

9. Y.Ji, J.A.Kilner, M.F.Carolan. Electrical conductivity and oxygen transfer in gadolium-doped ceria (CGO)-$CO_3O_{4-\delta}$ composites. *Journal of the European Ceramic Society* **24**(2004)3613-3616).

10. V. V. Kharton, A. P. Viskup, A. V. Kovalevsky, J. R. Jurado, E. N. Naumovich, A. A. Vecher, and J. R. Frade, "Oxygen ionic conductivity of Ti-containing strontium ferrite" *Solid State Ionics*, **133**, 57 2000.

11. D. P. Fagg, J. C. Waerenborgh, V. V. Kharton, and J. R. Frade,"Redox behavior and transport properties of $La_{0.5-x}Sr_{0.5-x}Fe_{0.4}Ti_{0.6}O_{3-\delta}$ ($0<x<0.1$) validated by Mössbauer spectroscopy", *Solid State Ionics*, **146**, 87-93, 2002.

12. D. P. Fagg, V. V. Kharton, J. R. Frade, A. A. L. Ferreira, "Stability and mixed ionic-electronic conductivity of (Sr,La)(Ti,Fe)O3-d perovskites", Solid state ionics. **156**, no. 1, (2003): 45-58.

13. P. Fagg, V. V. Kharton, A. V. Kovalevsky, A. P. Viskup, E. N. Naumovich, J. R. Frade, "The stability and mixed conductivity in La and Fe doped $SrTiO_3$ in the search for potential SOFC anode materials" *Journal of the European Ceramic Society.* **21**, no. 10-11, (2001): 1831-1835.

14. C.Y. Park and A.J. Jacobson, "Thermal and Chemical Expansion Properties of $La_{0.2}Sr_{0.8}Fe_{0.55}Ti_{0.45}O_{3-\delta,}$ " private communication 2006.

15. V. V. Kharton, F. M. Figueiredo, M A. P. Viskup, A. V. Kovalevsky, J. R. Jurado, L. Navarro, E. N. Naumovich, A. V. Kovalevsky, A. A. Yaremchenko, A. P. Viskup, A. Carneiro, F. M. B. Marques, and J. R. Frade, "Ceria-based materials for solid oxide fuel cells", *J. of Materials Sci.*, **36** (2001) 1105 – 1117.

16. K. Niihara, R. Morena and D.P.H. Hasselman, "Evaluation of K_{IC} of brittle solids by the indentation method with low crack-to-indent ratios", *J. Mater. Sci.Lett.*, **1**, 639-643 (1982).

17. S.Wang, E.Oikawa and T. Hashimoto, "Structural Analysis of $Ce_{1-x}M_xO_{2-0.5x-\delta}$ (M=Gd,Sm,Y) by High Tempearture XRD under Various Partial Pressures", " *J. Electochem. Soc.,* **151,** E46-E50 (2004)16.

18. X.-D. Zhou, Q. Cai, J. Yang, W.B. Yelon, W.J. James and H.U. Anderson, "Thermogravimetric analysis of LSFT as a function of pO_2 at elevated temperatures" Oxygen Transport Ceramic Membranes, DOE, Annual Report, p7, 2005

<u>Houston</u>

19. H. J. M. Bouwmeester, A. J. Burggraaf, "*The CRC Handbook of Solid State Electrochemistry*", Eds. P. J. Gellings and H. J. M. Bouwmeester, CRC Press, Boca Raton, (1997) 481.
20. J. Yoo, A. Verma, and A. J. Jacobson, Proc. Electrochem. Soc. PV2001-28 (2002) 27.
21. J. Yoo, A. Verma, S. Wang, and A. J. Jacobson, J. Electrochem. Soc. 152 (2005) A497.
22. C. Y. Park and A. J. Jacobson, J. Electrochem. Soc. 152 (2005) J65.
23. C. Y. Park and A. J. Jacobson, Solid State Ionics 176/35-36 (2005) 2671.
24. J. Yoo, C. Y. Park and A. J. Jacobson, Solid State Ionics 175(1-4) (2004) 55.